

# Vortex Line Topology in Iron-Based Superconductors with and without Second-Order Topology

Majid Kheirkhah,<sup>1,2</sup> Zhongbo Yan,<sup>1,\*</sup> and Frank Marsiglio<sup>2</sup>

<sup>1</sup>*School of Physics, Sun Yat-Sen University, Guangzhou 510275, China*

<sup>2</sup>*Department of Physics, University of Alberta, Edmonton, Alberta T6G 2E1, Canada*

(Dated: December 22, 2024)

The band topology of a superconductor is known to have profound impact on the existence of Majorana zero modes in vortices. Recently, experimental evidence of Majorana zero modes in vortices has been observed in iron-based superconductors with band inversion near the Fermi level. As iron-based superconductors with band inversion and  $s_{\pm}$ -wave pairing can give rise to second-order topological superconductivity, manifested by the presence of helical or chiral Majorana hinge states in three dimensions, we are motivated to investigate the potential impact of second-order topology on the vortex lines. We find when the second-order topology is absent, the vortex lines are topologically nontrivial in the weakly doped regime, with each end of the vortex lines binding one robust Majorana zero mode. On the other hand, when the second-order topology is present, the vortex lines are topologically trivial, with no Majorana zero modes appearing at their ends. Remarkably, we find that the presence of vortex lines can in turn lead to the appearance of Majorana zero modes on the hinges. By incorporating a realistic assumption of inhomogeneous superconductivity, the revealed strong interplay of second-order topology and vortex lines can explain the peculiar experimental observation of the coexistence of topologically nontrivial and trivial vortex lines in iron-based superconductors.

*Introduction.*— Topological superconductors (TSCs) and iron-based superconductors (FeSCs) have been two mainstays of the superconducting field for more than one decade. The great interest in TSCs lies in the various kinds of Majorana modes which hold promising applications in topological quantum computation [1–8]. For FeSCs, the great interest lies in their high superconducting transition temperature ( $T_c$ ), strongly correlated nature and pairing mechanisms leading to the emergence of unconventional pairings [9–14], such as the widely-known  $s_{\pm}$ -wave pairing [15, 16]. As FeSCs commonly have multiple bands near the Fermi energy, the possibility of the occurrence of band inversion with a realization of topological superconductivity through the Fu-Kane mechanism [5] has attracted considerable theoretical interest in the past few years [17–21]. Recently, several groups have experimentally observed that above  $T_c$ , band inversion occurs between the bands near the Fermi energy in a series of FeSCs, and below  $T_c$ , the surface Dirac cones associated with the inverted band structure are gapped by the bulk superconductivity [22–29]. The Fu-Kane mechanism is thus fulfilled in a single-material platform, unlike the various actively-studied heterostructures composed of different pieces of materials [30–34]. Therefore, the observation of compelling experimental evidence for vortex Majorana zero modes (MZMs) in FeSCs, like zero-bias peak with nearly quantized height and other ordered discrete peaks in the scanning tunneling spectroscopy [24–29], has generated tremendous interest [35–46]. Notably, in these FeSCs, topologically trivial vortex lines without MZMs are observed to coexist with topologically nontrivial vortex lines with MZMs [24–26, 47]. While mechanisms like pairing change induced by a Zeeman field or spatially dependent surface states have been proposed to

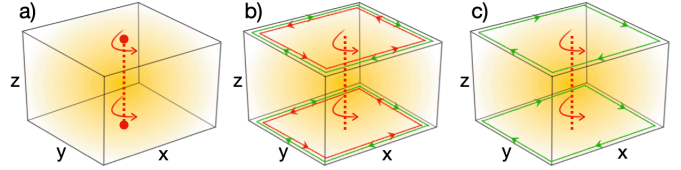


FIG. 1. (Color online) Schematic diagrams. (a) Each end of the  $z$  directional vortex line binds one robust Majorana zero mode (MZM) when the superconductor with band inversion is trivial in any order. (b)(c) The vortex line does not bind robust MZMs when the system is a second-order TSC with helical or chiral Majorana hinge modes.

explain this peculiar experimental finding [25, 42], a conclusive understanding is still far from established.

Another remarkable advance in TSCs is the recent birth of the concept named higher-order TSCs [48–85]. It is interesting that several theoretical works have revealed that a combination of inverted band structure and  $s_{\pm}$ -wave pairing can also give rise to second-order topological superconductivity [55, 56, 61], which is manifested by the presence of Majorana corner modes in two dimensions (2D) and Majorana hinge modes in 3D. Remarkably, experimental evidence for the existence of Majorana hinge modes in a 3D FeSC has also been reported [86]. These previous works motivate us to study the open question about the potential impact of second-order topology on the vortex lines in FeSCs. It is worth noting that while second-order TSCs can be realized in both 2D and 3D, we restrict ourselves to 3D in this work as these mentioned experiments were performed in bulk materials.

By focusing on the weakly doped regime relevant to the experiments, our main findings can be summarized as follows: (i) When the band topology of the 3D su-

perconductor is trivial, we find that the vortex lines are topologically nontrivial in the weakly doped regime, with each end of the vortex lines binding one robust MZM (see Fig. 1(a)), resembling the situation with conventional  $s$ -wave pairing [87]; (ii) When the system is a time-reversal invariant second-order TSC with helical Majorana hinge modes (see Fig. 1(b)), the vortex lines are trivial and do not bind MZMs at their ends. However, the introduction of vortex lines can gap out the helical Majorana hinge modes and result in MZMs on the hinges; (iii) When the system is driven into a time-reversal symmetry breaking second-order TSC with chiral Majorana hinge modes (see Fig. 1(c)) by a Zeeman field, the vortex lines still do not bind MZMs, but MZMs coexist with chiral Majorana modes on the hinges. These findings reveal that the second-order topology has a strong impact on the vortex-line topology.

*Theoretical formalism.*— The inverted band structure of iron-based superconductors near the Fermi level can be faithfully described by a four-band minimal model of 3D topological insulators [88, 89]. In combination with the  $s_{\pm}$ -wave pairing, the underlying physics can be described by the Bogoliubov-de Gennes Hamiltonian  $H = \frac{1}{2} \sum_{\mathbf{k}} \psi_{\mathbf{k}}^{\dagger} \mathcal{H}(\mathbf{k}) \psi_{\mathbf{k}}$ , where

$$\begin{aligned} \mathcal{H}(\mathbf{k}) = & m(\mathbf{k})\sigma_z s_0 \tau_z + 2\lambda \sum_{i=x,y,z} \sin k_i \sigma_x s_i \tau_z - \mu \sigma_0 s_0 \tau_z \\ & + \sigma_0 \mathbf{h} \cdot \mathbf{s} \tau_0 - \Delta(\mathbf{k}) \sigma_0 s_0 \tau_x, \end{aligned} \quad (1)$$

with the basis  $\psi_{\mathbf{k}}^{\text{T}} = (\mathbf{c}_{\mathbf{k}}, -i\sigma_0 s_y \mathbf{c}_{-\mathbf{k}}^{\dagger})$  where  $\mathbf{c}_{\mathbf{k}} = (c_{\mathbf{k},a,\uparrow}, c_{\mathbf{k},b,\uparrow}, c_{\mathbf{k},a,\downarrow}, c_{\mathbf{k},b,\downarrow})^{\text{T}}$ . For notational simplicity, the lattice constants are set to unity throughout this work. In Eq. (1), the Pauli matrices  $s_i$ ,  $\sigma_i$ , and  $\tau_i$  act on the spin ( $\uparrow, \downarrow$ ), orbital ( $a, b$ ), and particle-hole degrees of freedom, respectively, and  $s_0$ ,  $\sigma_0$ , and  $\tau_0$  are identity matrices.  $\lambda$  denotes the strength of spin-orbit coupling,  $\mu$  is the chemical potential, and  $\mathbf{h} = (h_x, h_y, h_z)$  denotes the Zeeman field, which is assumed to be present accompanying the generation of vortex lines. The  $m(\mathbf{k})$  term and the  $\Delta(\mathbf{k})$  term characterizes respectively the band inversion and the  $s_{\pm}$ -wave pairing, with their explicit forms given by

$$m(\mathbf{k}) = m_0 - 2t \sum_{i=x,y,z} \cos k_i, \quad (2)$$

$$\Delta(\mathbf{k}) = \Delta_0 + \Delta_s (\cos k_x + \cos k_y), \quad (3)$$

where  $t$  denotes the hopping amplitude. When the equal-energy contour  $m(\mathbf{k}) = 0$ , known as the band inversion surface (BIS), encloses a single time-reversal invariant momentum, the normal state hosts a topological gap and a single Dirac cone on each surface [90]. After becoming superconducting below  $T_c$ , the surface Dirac cones are gapped by the superconductivity. For a conventional  $s$ -wave pairing, *i.e.*,  $\Delta(\mathbf{k}) = \Delta_0$  in Eq. (3), it is known that its induced Dirac mass on the surfaces is uniform if the

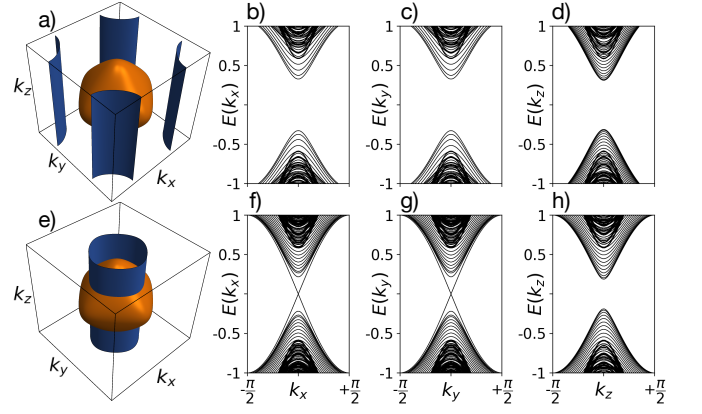


FIG. 2. (Color online) (a)-(d) No gapless modes appear on the hinges when the band inversion surface (BIS) and the pairing node surface (PNS) do not cross. (e)-(h) Helical Majorana modes appear on the hinges between  $z$ -normal surfaces and  $x$ - and  $y$ -normal surfaces when the BIS and PNS cross. Common parameters are:  $t = 1$ ,  $m_0 = 2.5$ ,  $\lambda = 0.5$ ,  $\mu = 0$ ,  $\mathbf{h} = 0$  and  $\Delta_0 = 0.25$ . (a)-(d)  $\Delta_s = 0.25$ , (e)-(h)  $\Delta_s = -0.25$ . The two directions with open boundary conditions are  $y$  and  $z$  in (b)(f),  $x$  and  $z$  in (c)(g), and  $x$  and  $y$  in (d)(h), and their lengths are 24 lattice spacings.

effect of disorder is negligible. In other words, there does not exist any kind of gapless boundary modes, indicating a trivial superconductor in any order. However, for the  $s_{\pm}$ -wave pairing given in Eq. (3), it has been shown in Ref. [61] that even though the first-order topology is trivial, nontrivial second-order topology, which is manifested by the presence of helical Majorana hinge modes, can be achieved in this system.

At  $\mu = 0$  and  $\mathbf{h} = 0$ , we can establish a simple geometric criterion for the realization of nontrivial second-order topology. The geometric picture of the criterion is the crossing of the BIS and the pairing node surface (PNS), which is the equal-energy contour  $\Delta(\mathbf{k}) = 0$ . The logic behind this geometric criterion is as follows. The Hamiltonian (1) at  $\mu = \mathbf{h} = 0$  can be divided into two parts, *i.e.*,  $H = H_e + H_o$ , where  $H_e$  and  $H_o$  represents respectively the even-parity and odd-parity part. Because  $\{H_e, H_o\} = 0$ , the even-parity part  $H_e$  plays the role of Dirac mass. When the energy spectra of  $H_e$  are gapless,  $H$  must be topologically nontrivial since the existence of nodes in  $H_e$  implies the existence of domain walls of Dirac mass on the boundary. Such kinds of geometric criteria are universally applicable to higher-order topological models as long as the condition that all terms of the Hamiltonian anticommute with each other is fulfilled [48, 49, 73].

To show the validity of the above geometric criterion explicitly, let us consider a cubic geometry with open boundary condition in two directions and periodic boundary condition in the remaining direction. As shown in the first row of Fig. 2, when the BIS and PNS do not cross

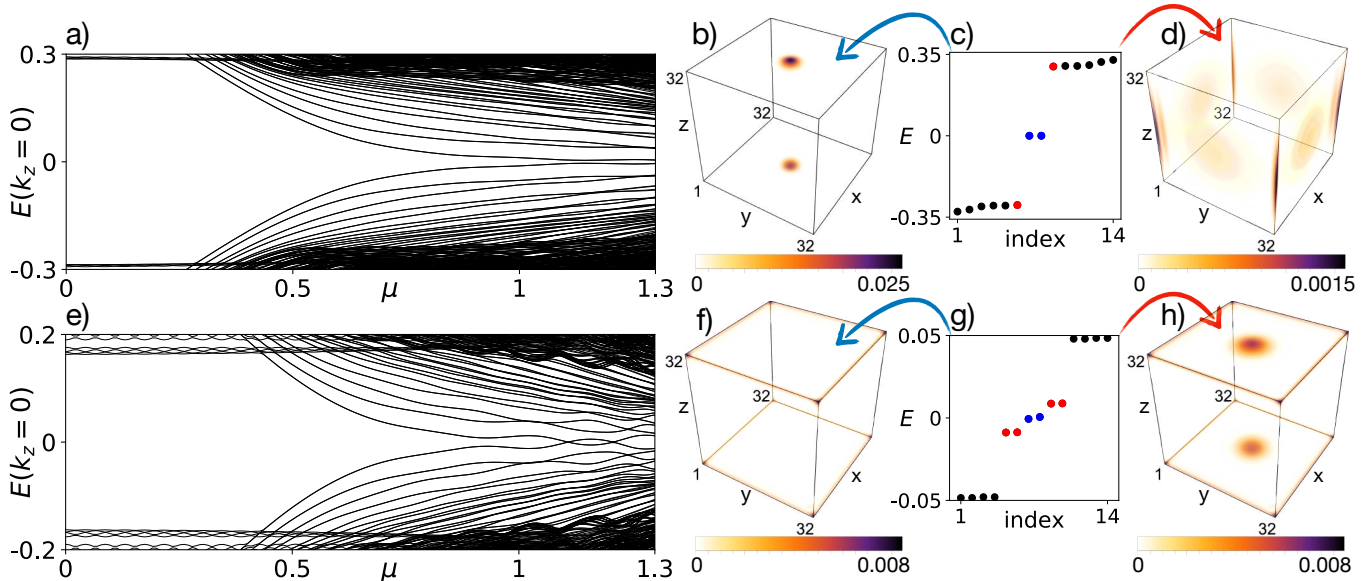


FIG. 3. (Color online) The evolution of energy dispersions at  $k_z = 0$  with respect to the doping level and the locations of MZMs. (a)-(d) and (e)-(h) show the results without and with second-order topology, respectively. For the parameters considered, the normal state becomes metallic when  $\mu > 0.5$ , and we restrict  $\mu < 1.3$  to guarantee the bulk spectrum to be gapped. In (a)(e), the lowest excitation spectrum shows a double degeneracy, and we find  $\nu = -1$  for the whole regime of  $\mu$  considered. It is noteworthy that because of the double degeneracy and  $\mathbb{Z}_2$  classification, the closures of energy gap near  $\mu = 1.2$  in (e) do not change  $\nu$ . In (c), the two blue dots correspond to two robust MZMs, and the two red dots correspond to high energy modes. (b) shows that the wave functions of the MZMs are strongly localized at the ends of the vortex line, and (d) shows that the two high energy modes correspond to gapped surface states. In (g), the two blue dots also correspond to two robust MZMs, and the four red dots correspond to splitting MZMs. (f) shows that the wave functions of the robust MZMs are localized on the hinges, and (h) shows that the wave functions of the four splitting MZMs are mostly localized at the ends of the vortex line. Common parameters are  $t = 1$ ,  $m_0 = 2.5$ ,  $\lambda = 0.5$ ,  $\mathbf{h} = 0$ ,  $\xi = 4$ , and  $\Delta_0 = 0.25$ . (a)-(d)  $\Delta_s = 0.25$ , (e)-(f)  $\Delta_s = -0.25$ , (a)(e)  $L_x = L_y = 32$ , and  $\mu = 0$ ,  $L_x = L_y = L_z = 32$  in (b)-(d) and (f)-(h).

(see the yellow and blue surfaces in Fig. 2(a)), there is no gapless hinge mode [Figs. 2(b)-2(d)], confirming the trivial topology. On the contrary, when the BIS and PNS cross, helical Majorana modes are found to appear on the interfacing hinges between  $z$ -normal surfaces and  $x$ - and  $y$ -normal surfaces [Figs. 2(f) and 2(g)], with their distributions the same as in Fig. 1(b).

When  $\mu$  or  $\mathbf{h}$  becomes nonzero, surely the above simple geometric criterion generally no longer holds because these two terms do not anticommute with all odd-parity terms in the Hamiltonian. Nevertheless, the second-order topology can survive even when the normal state becomes metallic (see Supplemental Material [91]). For the Zeeman field, while its introduction immediately breaks the time-reversal symmetry, we also find that the helical Majorana hinge modes shown in Figs. 2(f) and 2(g) are quite robust against it. Only when the Zeeman field becomes larger than a critical value, will the nature of the domain walls change and the helical Majorana hinge modes will become chiral Majorana hinge modes as illustrated in Fig. 1(c) (see more details in Supplemental Material [91]). Therefore, the simple Hamiltonian in Eq. (1) can realize both time-reversal invariant and chiral second-order TSCs.

*Interplay of second-order topology and vortex lines.*— In this work, we follow the experiments and focus on the configurations presented in Fig. 1, where the vortex lines are generated along the  $z$  direction. To illustrate the key physics in a clear way, we simplify the real situation with multiple vortex lines to an ideal situation with just a single  $\pi$ -flux vortex line. Such a simplification is justified in the weak-field regime, where the vortex lines are dilute and well-separated from each other. To simulate such a configuration, we assume that both on site and nearest-neighbor pairings follow such a spatial dependence,

$$\Delta_{0,s}(\mathbf{r}) = \Delta_{0,s} \tanh\left(\frac{\sqrt{x^2 + y^2}}{\xi}\right) \frac{x + iy}{\sqrt{x^2 + y^2}}, \quad (4)$$

where the core of the vortex is located at the lattice center of the  $xy$  plane,  $\xi$  is the superconducting coherence length, and  $(x, y)$  represents the coordinates of the lattice sites for on site pairing  $\Delta_0(\mathbf{r})$  and the coordinates of the lattice-bond centers for nearest-neighbor pairing  $\Delta_s(\mathbf{r})$  (see more details in the Supplemental Material [91]).

Since the vortex line breaks the time-reversal symmetry but preserves the translational symmetry in the  $z$  direction, the system can be viewed as a quasi-1D superconductor belonging to the class D of the Atland-Zirnbauer

classification [92, 93]. Accordingly, whether MZMs exist or not is characterized by a  $\mathbb{Z}_2$  invariant of the form [3, 91, 94]

$$\nu = \text{sgn}\{\text{Pf}[H_M(0)]\} \cdot \text{sgn}\{\text{Pf}[H_M(\pi)]\}, \quad (5)$$

where  $H_M(k_z)$  represents the Hamiltonian in the Majorana representation and ‘‘Pf’’ is a shorthand notation of Pfaffian (see more details in the Supplemental Material [91]).  $\nu = -1$  and  $+1$  indicates the presence and absence of one robust MZM at each end of the quasi-1D superconductor, respectively. The expression of the  $\mathbb{Z}_2$  invariant suggests that only the band information at the two time-reversal invariant momenta are important.

Let us first study the configuration in Fig. 2(a) for which the band topology of the homogeneous case is trivial in any order. Since the band inversion takes place at the  $\Gamma$  point, we only need to focus on the dispersion at  $k_z = 0$  in the weakly doped regime. From Fig. 3(a), we find that the lowest excitation spectrum shows a double degeneracy, which is distinct to the lowest excitation spectrum for  $s$ -wave pairing which is without degeneracy [87]. However, their topological properties are similar. That is, in the weakly doped regime (we only consider  $\mu > 0$  as the result is symmetric about  $\mu = 0$ ), we have  $\nu = -1$ , and each end of the vortex line binds one robust MZM, as shown in Figs. 3(b)-3(d).

Next let us study the configuration in Fig. 2(e) for which the second-order topology is nontrivial. We first consider that the Zeeman field is negligible, which can be a good approximation for materials with small  $g$  factor. From Fig. 3(e), it is readily seen that the double-degeneracy feature of the lowest excitation spectrum is also present. By calculating  $\nu$ , we also find  $\nu = -1$  in the weakly doped regime, indicating the existence of MZMs. However, the real-space results shown in Figs. 3(f)-3(h) reveal that the vortex line hosts two pairs of close-to-zero energy modes (see the red dots in Fig. 3(g)). With the results in the previous case and a local real-space picture in mind, the two pairs of modes should correspond to two pairs of MZMs whose energies, however, are split due to an overlap of wave functions, with one pair contributed by the well-known Fu-Kane mechanism, and the other pair contributed by the second-order topology. Since in class D the MZMs follow a  $\mathbb{Z}_2$  classification, *i.e.*, two overlapped MZMs is equivalent to a trivial fermion, the results indicate that the vortex line is trivialized by the second-order topology and no longer harbors robust MZMs at its ends. The above analysis about the vortex line is also supported by the finding of the presence of MZMs on the hinges. According to Figs. 3(f) and 3(g), we find that the introduction of a  $\pi$ -flux vortex line opens a small but finite energy gap to the helical Majorana hinge modes and leads to the formation of MZMs on the hinges.

With the results on the hinges in mind, we can go back to the vortex line and provide an intuitive picture to un-

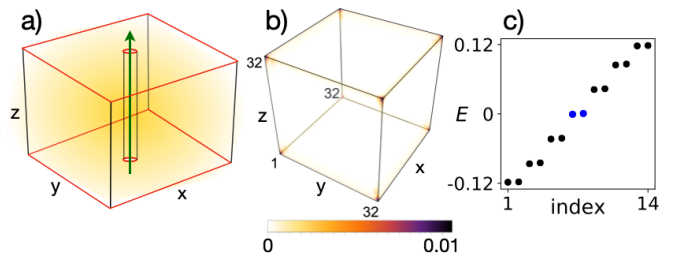


FIG. 4. (Color online) A schematic diagram to illustrate the emergence of domain walls at the vortex ends. The hinges and two circles in red color represent domain walls of Dirac mass induced by  $s_{\pm}$ -wave pairing and the vortex line. (b) shows that for a second-order TSC with chiral Majorana hinge modes, the wave functions of MZMs (two blue dots in (c)) are also localized on the hinges rather than at the vortex ends. We take  $t = 1$ ,  $m_0 = 2.5$ ,  $\lambda = 0.5$ ,  $\xi = 4$ ,  $h_z = 0.3$ ,  $h_x = h_y = 0$ ,  $\mu = 0$ ,  $\Delta_0 = -\Delta_s = 0.25$ , and  $L_x = L_y = L_z = 32$ .

derstand the origin of the pair of MZMs contributed by the second-order topology. The picture is as follows. As the superconducting order parameter vanishes at the vortex core, the effect of the vortex line is equivalent to creating an inner boundary of the cylinder form (Fig. 4(a)). Similarly to the outer surfaces, domain walls also form at the top and bottom circular boundaries of the inner cylinder surface, leading to the presence of an additional pair of MZMs which trivializes the vortex line.

Finally, we take the Zeeman field into account and study the situation with chiral Majorana hinge modes. As shown in Figs. 4(b) and 4(c), MZMs are also found to appear on the hinges, and the vortex line also does not bind robust MZMs. The trivialness of the vortex line can also be understood by following the picture illustrated in Fig. 4(a). As a final remark, it is worth noting that even though the top and bottom  $z$ -normal surfaces host one chiral Majorana modes on their edges, these two surfaces cannot be interpreted as 2D chiral superconductors with Chern number  $C = 1$ , because for the latter a  $\pi$ -flux vortex will bind one robust MZM[1].

*Discussions and Conclusions.*— Let us now apply our findings to explain the coexistence of topological and trivial vortex lines observed in experiment. We have shown that the criterion for second-order topology depends on the locations of both BIS and PNS. For  $s_{\pm}$ -wave pairing, the locations of PNS depend on the ratio  $\Delta_0/\Delta_s$ . As inhomogeneity is common in FeSCs,  $\Delta_0/\Delta_s$  should also be inhomogeneous in space. Assuming that  $\Delta_0/\Delta_s$  is almost a constant on a length scale comparable to the vortex size, then our results on the vortex line obtained in the clean limit can be applied. When the value of  $\Delta_0/\Delta_s$  in the concerned regions fulfills the criterion for second-order topology, vortex lines created in these regions will not host MZMs, and vice versa. In light of our findings, the experimental observation of the coexistence of topologically nontrivial and trivial vortices can

also be taken as a signature for the  $s_{\pm}$ -wave pairing in FeSCs.

In summary, the second-order topology and  $\pi$ -flux vortex lines show an intriguing interplay. Besides the FeSCs, this interplay is also worthy to study in other second-order topological superconductors of different origin.

*Acknowledgements.*— This work was supported in part by the Natural Sciences and Engineering Research Council of Canada (NSERC). Z.Y. is supported by Startup Grant of Sun Yat-sen University (No. 74130-18841219) and NSFC-11904417.

---

\* [yanzhhb5@mail.sysu.edu.cn](mailto:yanzhhb5@mail.sysu.edu.cn)

- [1] N. Read and Dmitry Green, “Paired states of fermions in two dimensions with breaking of parity and time-reversal symmetries and the fractional quantum Hall effect,” *Phys. Rev. B* **61**, 10267–10297 (2000).
- [2] D. A. Ivanov, “Non-abelian statistics of half-quantum vortices in  $p$ -wave superconductors,” *Phys. Rev. Lett.* **86**, 268–271 (2001).
- [3] Alexei Kitaev, “Unpaired Majorana fermions in quantum wires,” *Physics-Uspekhi* **44**, 131 (2001).
- [4] Chetan Nayak, Steven H. Simon, Ady Stern, Michael Freedman, and Sankar Das Sarma, “Non-abelian anyons and topological quantum computation,” *Rev. Mod. Phys.* **80**, 1083–1159 (2008).
- [5] Liang Fu and C. L. Kane, “Superconducting proximity effect and Majorana fermions at the surface of a topological insulator,” *Phys. Rev. Lett.* **100**, 096407 (2008).
- [6] Roman M. Lutchyn, Jay D. Sau, and S. Das Sarma, “Majorana fermions and a topological phase transition in semiconductor-superconductor heterostructures,” *Phys. Rev. Lett.* **105**, 077001 (2010).
- [7] Yuval Oreg, Gil Refael, and Felix von Oppen, “Helical liquids and Majorana bound states in quantum wires,” *Phys. Rev. Lett.* **105**, 177002 (2010).
- [8] Jason Alicea, Yuval Oreg, Gil Refael, Felix von Oppen, and Matthew P. A. Fisher, “Non-abelian statistics and topological quantum information processing in 1D wire networks,” *Nature Physics* **7**, 412–417 (2011).
- [9] Johnpierre Paglione and Richard L. Greene, “High-temperature superconductivity in iron-based materials,” *Nature Physics* **6**, 645–658 (2010).
- [10] P J Hirschfeld, M M Korshunov, and I I Mazin, “Gap symmetry and structure of Fe-based superconductors,” *Reports on Progress in Physics* **74**, 124508 (2011).
- [11] G. R. Stewart, “Superconductivity in iron compounds,” *Rev. Mod. Phys.* **83**, 1589–1652 (2011).
- [12] Andrey Chubukov, “Pairing mechanism in Fe-based superconductors,” *Annual Review of Condensed Matter Physics* **3**, 57–92 (2012).
- [13] Elbio Dagotto, “Colloquium: The unexpected properties of alkali metal iron selenide superconductors,” *Rev. Mod. Phys.* **85**, 849–867 (2013).
- [14] Pengcheng Dai, “Antiferromagnetic order and spin dynamics in iron-based superconductors,” *Rev. Mod. Phys.* **87**, 855–896 (2015).
- [15] I. I. Mazin, D. J. Singh, M. D. Johannes, and M. H. Du, “Unconventional superconductivity with a sign reversal in the order parameter of  $\text{LaFeAsO}_{1-x}\text{F}_x$ ,” *Phys. Rev. Lett.* **101**, 057003 (2008).
- [16] Fa Wang and Dung-Hai Lee, “The electron-pairing mechanism of iron-based superconductors,” *Science* **332**, 200–204 (2011).
- [17] Zhijun Wang, P. Zhang, Gang Xu, L. K. Zeng, H. Miao, Xiaoyan Xu, T. Qian, Hongming Weng, P. Richard, A. V. Fedorov, H. Ding, Xi Dai, and Zhong Fang, “Topological nature of the  $\text{FeSe}_{0.5}\text{Te}_{0.5}$  superconductor,” *Phys. Rev. B* **92**, 115119 (2015).
- [18] Xianxin Wu, Shengshan Qin, Yi Liang, Heng Fan, and Jiangping Hu, “Topological characters in  $\text{Fe}(\text{Te}_{1-x}\text{Se}_x)$  thin films,” *Phys. Rev. B* **93**, 115129 (2016).
- [19] Gang Xu, Biao Lian, Peizhe Tang, Xiao-Liang Qi, and Shou-Cheng Zhang, “Topological superconductivity on the surface of Fe-based superconductors,” *Phys. Rev. Lett.* **117**, 047001 (2016).
- [20] Ning Hao and Jiangping Hu, “Topological quantum states of matter in iron-based superconductors: from concept to material realization,” *National Science Review* **6**, 213–226 (2019).
- [21] Andreas Kreisel, PJ Hirschfeld, and Brian M Andersen, “On the Remarkable Superconductivity of FeSe and its Close Cousins,” *arXiv preprint arXiv:2007.02966* (2020).
- [22] Peng Zhang, Koichiro Yaji, Takahiro Hashimoto, Yuichi Ota, Takeshi Kondo, Kozo Okazaki, Zhijun Wang, Jincheng Wen, GD Gu, Hong Ding, *et al.*, “Observation of topological superconductivity on the surface of an iron-based superconductor,” *Science* **360**, 182–186 (2018).
- [23] Peng Zhang, Zhijun Wang, Xianxin Wu, Koichiro Yaji, Yukiaki Ishida, Yoshimitsu Kohama, Guangyang Dai, Yue Sun, Cedric Bareille, Kenta Kuroda, *et al.*, “Multiple topological states in iron-based superconductors,” *Nature Physics* **15**, 41 (2019).
- [24] Dongfei Wang, Lingyuan Kong, Peng Fan, Hui Chen, Shiyu Zhu, Wenyao Liu, Lu Cao, Yujie Sun, Shixuan Du, John Schneeloch, *et al.*, “Evidence for Majorana bound states in an iron-based superconductor,” *Science* **362**, 333–335 (2018).
- [25] Lingyuan Kong, Shiyu Zhu, Michał Papaj, Hui Chen, Lu Cao, Hiroki Isobe, Yuqing Xing, Wenyao Liu, Dongfei Wang, Peng Fan, *et al.*, “Half-integer level shift of vortex bound states in an iron-based superconductor,” *Nature Physics* , 1–7 (2019).
- [26] T Machida, Y Sun, S Pyon, S Takeda, Y Kohsaka, T Hanaguri, T Sasagawa, and T Tamegai, “Zero-energy vortex bound state in the superconducting topological surface state of Fe (Se, Te),” *Nature materials* , 1 (2019).
- [27] Qin Liu, Chen Chen, Tong Zhang, Rui Peng, Ya-Jun Yan, Chen-Hao-Ping Wen, Xia Lou, Yu-Long Huang, Jin-Peng Tian, Xiao-Li Dong, Guang-Wei Wang, Wei-Cheng Bao, Qiang-Hua Wang, Zhi-Ping Yin, Zhong-Xian Zhao, and Dong-Lai Feng, “Robust and clean Majorana zero mode in the vortex core of high-temperature superconductor  $(\text{Li}_{0.84}\text{Fe}_{0.16})\text{OHFeSe}$ ,” *Phys. Rev. X* **8**, 041056 (2018).
- [28] C Chen, Q Liu, TZ Zhang, D Li, PP Shen, XL Dong, Z-X Zhao, T Zhang, and DL Feng, “Quantized conductance of Majorana zero mode in the vortex of the topological superconductor  $(\text{Li}_{0.84}\text{Fe}_{0.16})\text{OHFeSe}$ ,” *Chinese Physics Letters* **36**, 057403 (2019).
- [29] Shiyu Zhu, Lingyuan Kong, Lu Cao, Hui Chen, Michał Papaj, Shixuan Du, Yuqing Xing, Wenyao Liu, Dongfei Wang, Chengmin Shen, Fazhi Yang, John Schneeloch, Ruidan Zhong, Genda Gu, Liang Fu, Yu-Yang Zhang,

- Hong Ding, and Hong-Jun Gao, “Nearly quantized conductance plateau of vortex zero mode in an iron-based superconductor,” *Science* **367**, 189–192 (2020).
- [30] V. Mourik, K. Zuo, S. M. Frolov, S. R. Plissard, E. P. A. M. Bakkers, and L. P. Kouwenhoven, “Signatures of Majorana fermions in hybrid superconductor-semiconductor nanowire devices,” *Science* **336**, 1003–1007 (2012).
- [31] Stevan Nadj-Perge, Ilya K. Drozdov, Jian Li, Hua Chen, Sangjun Jeon, Jungpil Seo, Allan H. MacDonald, B. Andrei Bernevig, and Ali Yazdani, “Observation of Majorana fermions in ferromagnetic atomic chains on a superconductor,” *Science* **346**, 602–607 (2014).
- [32] Hao-Hua Sun, Kai-Wen Zhang, Lun-Hui Hu, Chuang Li, Guan-Yong Wang, Hai-Yang Ma, Zhu-An Xu, Chun-Lei Gao, Dan-Dan Guan, Yao-Yi Li, Canhua Liu, Dong Qian, Yi Zhou, Liang Fu, Shao-Chun Li, Fu-Chun Zhang, and Jin-Feng Jia, “Majorana zero mode detected with spin selective Andreev reflection in the vortex of a topological superconductor,” *Phys. Rev. Lett.* **116**, 257003 (2016).
- [33] Hao Zhang, Chun-Xiao Liu, Sasa Gazibegovic, Di Xu, John A Logan, Guanzhong Wang, Nick van Loo, Jouri DS Bommer, Michiel WA de Moor, Diana Car, Roy L. M. Op het Veld, Petrus J. van Veldhoven, Sebastian Koelling, Marcel A. Verheijen, Mihir Pendharkar, Daniel J. Pennachio, Borzoyeh Shojaei, Joon Sue Lee, Chris J. Palmstrm, Erik P. A. M. Bakkers, S. Das Sarma, and Leo P. Kouwenhoven, “Quantized Majorana conductance,” *Nature* **556**, 74 (2018).
- [34] Antonio Fornieri, Alexander M. Whiticar, F. Setiawan, Elías Portolés, Asbjørn C. C. Drachmann, Anna Keselman, Sergei Gronin, Candice Thomas, Tian Wang, Ray Kallaher, Geoffrey C. Gardner, Erez Berg, Michael J. Manfra, Ady Stern, Charles M. Marcus, and Fabrizio Nichele, “Evidence of topological superconductivity in planar Josephson junctions,” *Nature* **569**, 89–92 (2019).
- [35] Kun Jiang, Xi Dai, and Ziqiang Wang, “Quantum anomalous vortex and Majorana zero mode in iron-based superconductor Fe(Te,Se),” *Phys. Rev. X* **9**, 011033 (2019).
- [36] X.-L. Peng, Y. Li, X.-X. Wu, H.-B. Deng, X. Shi, W.-H. Fan, M. Li, Y.-B. Huang, T. Qian, P. Richard, J.-P. Hu, S.-H. Pan, H.-Q. Mao, Y.-J. Sun, and H. Ding, “Observation of topological transition in high- $T_c$  superconducting monolayer FeTe $_{1-x}$ Se $_x$  films on SrTiO $_3$ (001),” *Phys. Rev. B* **100**, 155134 (2019).
- [37] Ching-Kai Chiu, T Machida, Yingyi Huang, T Hanaguri, and Fu-Chun Zhang, “Scalable Majorana vortex modes in iron-based superconductors,” *Science Advances* **6**, eaay0443 (2020).
- [38] Zhenyu Wang, Jorge Olivares Rodriguez, Lin Jiao, Sean Howard, Martin Graham, G. D. Gu, Taylor L. Hughes, Dirk K. Morr, and Vidya Madhavan, “Evidence for dispersing 1D Majorana channels in an iron-based superconductor,” *Science* **367**, 104–108 (2020).
- [39] Cheng Chen, Kun Jiang, Yi Zhang, Chaofei Liu, Yi Liu, Ziqiang Wang, and Jian Wang, “Atomic line defects and zero-energy end states in monolayer Fe(Te,Se) high-temperature superconductors,” *Nature Physics* **16**, 536–540 (2020).
- [40] Yi Zhang, Kun Jiang, Fuchun Zhang, Jian Wang, and Ziqiang Wang, “Atomic line defects in unconventional superconductors as a new route toward one dimensional topological superconductors,” [arXiv preprint arXiv:2004.05860](#) (2020).
- [41] Xianxin Wu, Jia-Xin Yin, Chao-Xing Liu, and Jiangping Hu, “Topological magnetic line defects in Fe(Te, Se) high-temperature superconductors,” [arXiv preprint arXiv:2004.05848](#) (2020).
- [42] Areg Ghazaryan, P. L. S. Lopes, Pavan Hosur, Matthew J. Gilbert, and Pouyan Ghaemi, “Effect of zeeman coupling on the Majorana vortex modes in iron-based topological superconductors,” *Phys. Rev. B* **101**, 020504 (2020).
- [43] Shengshan Qin, Lunhui Hu, Congcong Le, Jinfeng Zeng, Fu-chun Zhang, Chen Fang, and Jiangping Hu, “Quasi-1D topological nodal vortex line phase in doped superconducting 3D Dirac semimetals,” *Phys. Rev. Lett.* **123**, 027003 (2019).
- [44] Shengshan Qin, Lunhui Hu, Xianxin Wu, Xia Dai, Chen Fang, Fu-Chun Zhang, and Jiangping Hu, “Topological vortex phase transitions in iron-based superconductors,” *Science Bulletin* **64**, 1207 – 1214 (2019).
- [45] Elio J. König and Piers Coleman, “Crystalline-symmetry-protected helical Majorana modes in the Iron Pnictides,” *Phys. Rev. Lett.* **122**, 207001 (2019).
- [46] Zhongbo Yan, Zhigang Wu, and Wen Huang, “Vortex end Majorana zero modes in superconducting Dirac and Weyl semimetals,” *Phys. Rev. Lett.* **124**, 257001 (2020).
- [47] Mingyang Chen, Xiaoyu Chen, Huan Yang, Zengyi Du, Xiyu Zhu, Enyu Wang, and Hai-Hu Wen, “Discrete energy levels of Caroli-de Gennes-Matricon states in quantum limit in FeTe $_{0.55}$ Se $_{0.45}$ ,” *Nature Communications* **9**, 970 (2018).
- [48] Wladimir A. Benalcazar, B. Andrei Bernevig, and Taylor L. Hughes, “Quantized electric multipole insulators,” *Science* **357**, 61–66 (2017).
- [49] Frank Schindler, Ashley M. Cook, Maia G. Vergniory, Zhijun Wang, Stuart S. P. Parkin, B. Andrei Bernevig, and Titus Neupert, “Higher-order topological insulators,” *Science Advances* **4** (2018), 10.1126/sciadv.aat0346.
- [50] Josias Langbehn, Yang Peng, Luka Trifunovic, Felix von Oppen, and Piet W. Brouwer, “Reflection-symmetric second-order topological insulators and superconductors,” *Phys. Rev. Lett.* **119**, 246401 (2017).
- [51] Hassan Shapourian, Yuxuan Wang, and Shinsei Ryu, “Topological crystalline superconductivity and second-order topological superconductivity in nodal-loop materials,” *Phys. Rev. B* **97**, 094508 (2018).
- [52] Eslam Khalaf, “Higher-order topological insulators and superconductors protected by inversion symmetry,” *Phys. Rev. B* **97**, 205136 (2018).
- [53] Max Geier, Luka Trifunovic, Max Hoskam, and Piet W. Brouwer, “Second-order topological insulators and superconductors with an order-two crystalline symmetry,” *Phys. Rev. B* **97**, 205135 (2018).
- [54] Xiaoyu Zhu, “Tunable Majorana corner states in a two-dimensional second-order topological superconductor induced by magnetic fields,” *Phys. Rev. B* **97**, 205134 (2018).
- [55] Zhongbo Yan, Fei Song, and Zhong Wang, “Majorana corner modes in a high-temperature platform,” *Phys. Rev. Lett.* **121**, 096803 (2018).
- [56] Qiyue Wang, Cheng-Cheng Liu, Yuan-Ming Lu, and Fan Zhang, “High-temperature Majorana corner states,” *Phys. Rev. Lett.* **121**, 186801 (2018).

- [57] Yuxuan Wang, Mao Lin, and Taylor L. Hughes, “Weak-pairing higher order topological superconductors,” *Phys. Rev. B* **98**, 165144 (2018).
- [58] Chen-Hsuan Hsu, Peter Stano, Jelena Klinovaja, and Daniel Loss, “Majorana Kramers pairs in higher-order topological insulators,” *Phys. Rev. Lett.* **121**, 196801 (2018).
- [59] Tao Liu, James Jun He, and Franco Nori, “Majorana corner states in a two-dimensional magnetic topological insulator on a high-temperature superconductor,” *Phys. Rev. B* **98**, 245413 (2018).
- [60] Zhigang Wu, Zhongbo Yan, and Wen Huang, “Higher-order topological superconductivity: Possible realization in Fermi gases and  $\text{Sr}_2\text{RuO}_4$ ,” *Phys. Rev. B* **99**, 020508 (2019).
- [61] Rui-Xing Zhang, William S. Cole, and S. Das Sarma, “Helical hinge Majorana modes in iron-based superconductors,” *Phys. Rev. Lett.* **122**, 187001 (2019).
- [62] Yanick Volpez, Daniel Loss, and Jelena Klinovaja, “Second-order topological superconductivity in  $\pi$ -junction Rashba layers,” *Phys. Rev. Lett.* **122**, 126402 (2019).
- [63] Rui-Xing Zhang, William S. Cole, Xianxin Wu, and S. Das Sarma, “Higher-order topology and nodal topological superconductivity in Fe(Se,Te) heterostructures,” *Phys. Rev. Lett.* **123**, 167001 (2019).
- [64] Xianxin Wu, Xin Liu, Ronny Thomale, and Chao-Xing Liu, “High- $T_c$  Superconductor Fe(Se,Te) Monolayer: an Intrinsic, Scalable and Electrically-tunable Majorana Platform,” *arXiv preprint arXiv:1905.10648* (2019).
- [65] Yi-Ting Hsu, William S Cole, Rui-Xing Zhang, and Jay D Sau, “Inversion-protected higher order topological superconductivity in monolayer  $\text{WTe}_2$ ,” *arXiv preprint arXiv:1904.06361* (2019).
- [66] Chuanchang Zeng, T. D. Stanescu, Chuanwei Zhang, V. W. Scarola, and Sumanta Tewari, “Majorana corner modes with solitons in an attractive Hubbard-Hofstadter model of cold atom optical lattices,” *Phys. Rev. Lett.* **123**, 060402 (2019).
- [67] Nick Bultinck, B. Andrei Bernevig, and Michael P. Zaletel, “Three-dimensional superconductors with hybrid higher-order topology,” *Phys. Rev. B* **99**, 125149 (2019).
- [68] Sayed Ali Akbar Ghorashi, Xiang Hu, Taylor L. Hughes, and Enrico Rossi, “Second-order Dirac superconductors and magnetic field induced Majorana hinge modes,” *Phys. Rev. B* **100**, 020509 (2019).
- [69] Yang Peng and Yong Xu, “Proximity-induced Majorana hinge modes in antiferromagnetic topological insulators,” *Phys. Rev. B* **99**, 195431 (2019).
- [70] Xiaoyu Zhu, “Second-order topological superconductors with mixed pairing,” *Phys. Rev. Lett.* **122**, 236401 (2019).
- [71] Katharina Laubscher, Daniel Loss, and Jelena Klinovaja, “Fractional topological superconductivity and parafermion corner states,” *Phys. Rev. Research* **1**, 032017 (2019).
- [72] Xiao-Hong Pan, Kai-Jie Yang, Li Chen, Gang Xu, Chao-Xing Liu, and Xin Liu, “Lattice-symmetry-assisted second-order topological superconductors and Majorana patterns,” *Phys. Rev. Lett.* **123**, 156801 (2019).
- [73] Zhongbo Yan, “Higher-order topological odd-parity superconductors,” *Phys. Rev. Lett.* **123**, 177001 (2019).
- [74] Zhongbo Yan, “Majorana corner and hinge modes in second-order topological insulator/superconductor heterostructures,” *Phys. Rev. B* **100**, 205406 (2019).
- [75] S. Franca, D. V. Efremov, and I. C. Fulga, “Phase-tunable second-order topological superconductor,” *Phys. Rev. B* **100**, 075415 (2019).
- [76] Majid Kheirkhah, Yuki Nagai, Chun Chen, and Frank Marsiglio, “Majorana corner flat bands in two-dimensional second-order topological superconductors,” *Phys. Rev. B* **101**, 104502 (2020).
- [77] Song-Bo Zhang and Björn Trauzettel, “Detection of second-order topological superconductors by Josephson junctions,” *Phys. Rev. Research* **2**, 012018 (2020).
- [78] Junyeong Ahn and Bohm-Jung Yang, “Higher-order topological superconductivity of spin-polarized fermions,” *Phys. Rev. Research* **2**, 012060 (2020).
- [79] Suman Jyoti De, Udit Khanna, and Sumathi Rao, “Magnetic flux periodicity in second order topological superconductors,” *Phys. Rev. B* **101**, 125429 (2020).
- [80] Bitan Roy, “Higher-order topological superconductors in  $\mathcal{P}$ -,  $\mathcal{T}$ -odd quadrupolar Dirac materials,” *Phys. Rev. B* **101**, 220506 (2020).
- [81] Ya-Jie Wu, Junpeng Hou, Yun-Mei Li, Xi-Wang Luo, Xiaoyan Shi, and Chuanwei Zhang, “In-plane Zeeman-field-induced Majorana corner and hinge modes in an s-wave superconductor heterostructure,” *Phys. Rev. Lett.* **124**, 227001 (2020).
- [82] Majid Kheirkhah, Zhongbo Yan, Yuki Nagai, and Frank Marsiglio, “First- and second-order topological superconductivity and temperature-driven topological phase transitions in the extended Hubbard model with spin-orbit coupling,” *Phys. Rev. Lett.* **125**, 017001 (2020).
- [83] Sayed Ali Akbar Ghorashi, Taylor L. Hughes, and Enrico Rossi, “Vortex and surface phase transitions in superconducting higher-order topological insulators,” *Phys. Rev. Lett.* **125**, 037001 (2020).
- [84] Li Chen, Bin Liu, Gang Xu, and Xin Liu, “Lattice distortion induced first and second order topological phase transition in rectangular high- $T_c$  superconducting monolayer,” *arXiv preprint arXiv:1909.10402* (2019).
- [85] Jingjing Niu, Tongxing Yan, Yuxuan Zhou, Ziyu Tao, Xiaole Li, Weiyang Liu, Libo Zhang, Song Liu, Zhongbo Yan, Yuanzhen Chen, *et al.*, “Simulation of Higher-Order Topological Phases and Related Topological Phase Transitions in a Superconducting Qubit,” *arXiv preprint arXiv:2001.03933* (2020).
- [86] Mason J. Gray, Josef Freudenstein, Shu Yang F. Zhao, Ryan OConnor, Samuel Jenkins, Narendra Kumar, Marcel Hoek, Abigail Kopec, Soonsang Huh, Takashi Taniguchi, Kenji Watanabe, Ruidan Zhong, Changyoung Kim, G. D. Gu, and K. S. Burch, “Evidence for helical hinge zero modes in an Fe-based superconductor,” *Nano Letters* **19**, 4890–4896 (2019).
- [87] Pavan Hosur, Pouyan Ghaemi, Roger S. K. Mong, and Ashvin Vishwanath, “Majorana modes at the ends of superconductor vortices in doped topological insulators,” *Phys. Rev. Lett.* **107**, 097001 (2011).
- [88] M Zahid Hasan and Charles L Kane, “Colloquium: topological insulators,” *Reviews of Modern Physics* **82**, 3045 (2010).
- [89] Xiao-Liang Qi and Shou-Cheng Zhang, “Topological insulators and superconductors,” *Reviews of Modern Physics* **83**, 1057 (2011).

- [90] Liang Fu and C. L. Kane, “Topological insulators with inversion symmetry,” [PRB \*\*76\*\*, 045302 \(2007\)](#).
- [91] See Supplemental Material for details of calculations.
- [92] Andreas P. Schnyder, Shinsei Ryu, Akira Furusaki, and Andreas W. W. Ludwig, “Classification of topological insulators and superconductors in three spatial dimensions,” [Phys. Rev. B \*\*78\*\*, 195125 \(2008\)](#).
- [93] Alexei Kitaev, “Periodic table for topological insulators and superconductors,” in [AIP Conference Proceedings](#), Vol. 1134 (AIP, 2009) pp. 22–30.
- [94] M. Wimmer, “Algorithm 923: Efficient numerical computation of the Pfaffian for dense and banded skew-symmetric matrices,” [ACM Trans. Math. Softw. \*\*38\*\*, 30:1–30:17 \(2012\)](#).

# Supplemental Material for “Vortex Line Topology in Iron-Based Superconductors with and without Second-Order Topology”

Majid Kheirkhah,<sup>1,2</sup> Zhongbo Yan,<sup>1,\*</sup> and Frank Marsiglio<sup>2</sup>

<sup>1</sup>*School of Physics, Sun Yat-Sen University, Guangzhou 510275, China*

<sup>2</sup>*Department of Physics, University of Alberta, Edmonton, Alberta T6G 2E1, Canada*

This supplemental material provides the details of the derivations of some important equations presented in the main text. It consists of six sections: (I) Phase diagram; (II) Real space BdG Hamiltonian; (III) The  $\mathbb{Z}_2$  invariant characterizes the system; (IV) The effects of Zeeman field on the helical Majorana hinge modes; (V) Vortex lines in the  $x$  direction; (VI) Helical and chiral Majorana hinge modes for a finite-size cubic sample in the absence of vortex lines.

## I. PHASE DIAGRAM

In momentum space, the minimal BdG Hamiltonian for iron-based superconductors with band inversion can be written as

$$\mathcal{H} = \frac{1}{2} \sum_{\mathbf{k}} \begin{pmatrix} c_{\mathbf{k}}^\dagger & c_{-\mathbf{k}} \end{pmatrix} \begin{pmatrix} H_0(\mathbf{k}) & \Delta(\mathbf{k}) \\ \Delta^\dagger(\mathbf{k}) & -H_0^*(-\mathbf{k}) \end{pmatrix} \begin{pmatrix} c_{\mathbf{k}} \\ c_{-\mathbf{k}}^\dagger \end{pmatrix}, \quad (\text{S1})$$

where  $\mathbf{c}_{\mathbf{k}} = (c_{\mathbf{k},a,\uparrow}, c_{\mathbf{k},b,\uparrow}, c_{\mathbf{k},a,\downarrow}, c_{\mathbf{k},b,\downarrow})^T$  and

$$H_0(\mathbf{k}) = (m_0 - 2t \sum_{i=x,y,z} \cos k_i) \sigma_z s_0 + 2\lambda \sum_{i=x,y,z} \sin k_i \sigma_x s_i - \mu \sigma_0 s_0 + \sigma_0 \mathbf{h} \cdot \mathbf{s}, \quad (\text{S2})$$

$$\Delta(\mathbf{k}) = i \{ \Delta_0 + \Delta_s (\cos k_x + \cos k_y) \} \sigma_0 s_y. \quad (\text{S3})$$

Here,  $\mathbf{h} = (h_x, h_y, h_z)$ ,  $\mathbf{s} = (s_x, s_y, s_z)$ , and the Pauli matrices  $\sigma$  and  $s$  act in orbital ( $a, b$ ) and spin ( $\uparrow, \downarrow$ ) degrees of freedom, respectively, and  $\sigma_0$  and  $s_0$  are the unit matrices.  $H_0(\mathbf{k})$  describes the normal state, and  $\Delta(\mathbf{k})$  represents the  $s_{\pm}$ -wave pairing. In this section, we focus on the uniform case without vortex lines and Zeeman field. Throughout the main text, we have chosen  $t = 1$  as the unit of energy,  $m_0 = 2.5$ ,  $\lambda = 0.5$ , so that a band inversion takes place at the  $\Gamma = (0, 0, 0)$ . It is worth noting that for this set of parameters, the band edges are located at  $(0, \pi, 0)$  and  $(\pi, 0, 0)$ , with the energy gap  $E_g = 1.0$ . The normal state becomes metallic when  $\mu > 0.5$  (we only consider positive  $\mu$  because the results are symmetric about  $\mu = 0$ ). After becoming superconducting, the doubly degenerate eigenvalues of the BdG Hamiltonian for  $\mathbf{h} = 0$  are given by,

$$E_{(\pm, \pm)}(\mathbf{k}) = \pm \sqrt{\varepsilon_{\pm}^2(\mathbf{k}) + \Delta^2(\mathbf{k})}, \quad (\text{S4})$$

where

$$\varepsilon_{\pm}(\mathbf{k}) = \mu \pm \sqrt{(m_0 - 2t \sum_{i=x,y,z} \cos k_i)^2 + 4\lambda^2 \sum_{i=x,y,z} \sin^2 k_i}. \quad (\text{S5})$$

Because  $s_{\pm}$ -wave pairing has nodes when  $|\Delta_0| < 2|\Delta_s|$ , the superconductor can be gapless when the Fermi surface intersects with the pairing nodes. As the location of pairing nodes is determined by  $\Delta(\mathbf{k}) = 0$ , and the location of Fermi surface is determined by  $\varepsilon_{-}(\mathbf{k}) = 0$ , we can numerically determine the phase boundary which separates the gapped phase from the gapless phase by checking when the contour for  $\Delta(\mathbf{k}) = 0$  intersects with the contour for  $\varepsilon_{-}(\mathbf{k}) = 0$ . The phase boundary is shown in Fig. S1.

As the energy bands of the concerned iron-based superconductors are gapped, therefore, in this work we are interested in the gapped regime. Within the gapped regime, the phase can be further divided as second-order topological superconductor and trivial superconductor. At  $\mu = 0$ , we have pointed out in the main text that when the band inversion surface and pairing node surface cross, the system is a second-order topological superconductor with helical Majorana hinge modes. If we start with the crossing case, it is expected that a transition from the second-order topological superconducting phase to the trivial superconducting phase should happen. It is known that

a topological phase transition from a first-order topological phase to a trivial phase is always associated with the closure of the bulk energy gap as long as the symmetry class does not change. However, a topological phase transition from a second-order topological phase to a trivial phase in general does not require the closure of the bulk energy gap; what it requires is the closure of the energy gap of the surface states. Interestingly, for the set of isotropic parameters considered in this work, we found that the closure of surface energy gap coincides with the closure of the bulk energy gap, indicating that the phase boundary of the second-order topological superconducting phase with a finite bulk gap coincides with the gapped-gapless phase boundary. These findings establish the phase diagram in Fig. S1.

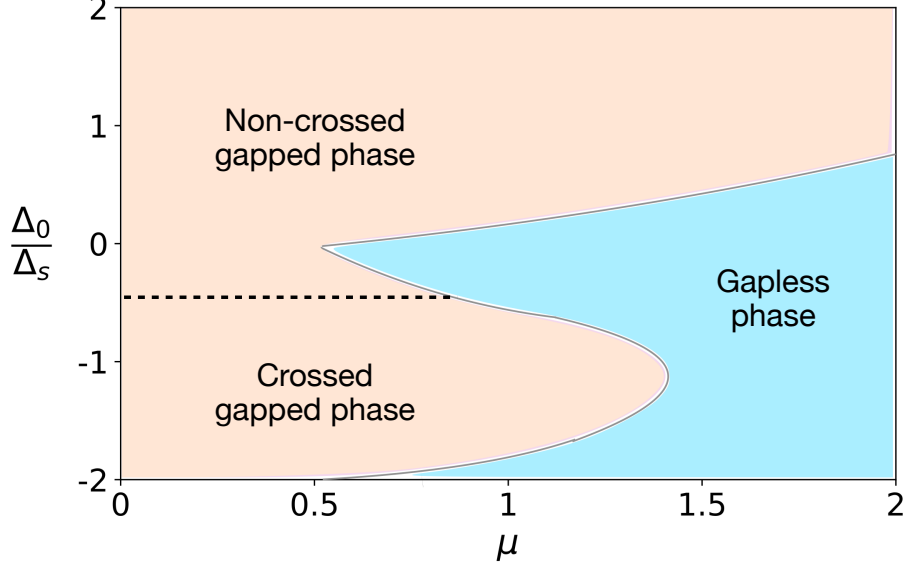


FIG. S1. (Color online) The phase diagram consists of gapped (orange region) and gapless (blue region) phases. We take  $t = 1$ ,  $m_0 = 2.5$ ,  $\lambda = 0.5$ , and  $\mathbf{h} = 0$ . The horizontal dashed line divides the gapped phase into two distinct topological phases. The crossed gapped phase corresponds to a gapped second-order topological superconducting phase with the underlying band inversion surface and pairing node surface crossing with each other. The noncrossed gapped phase corresponds to a gapped trivial superconducting phase with the underlying band inversion surface and pairing node surface separated in the Brillouin zone.

## II. REAL SPACE BDG HAMILTONIAN

According to the BdG Hamiltonian in momentum space, the real space Hamiltonian is obtained as

$$H = \frac{1}{2} \sum_{i,j} (\mathbf{c}_i^\dagger, \mathbf{c}_i) \begin{pmatrix} H_{0;ij} & \Delta_{ij} \\ -\Delta_{ij}^* & -H_{0;ij}^* \end{pmatrix} \begin{pmatrix} \mathbf{c}_j \\ \mathbf{c}_j^\dagger \end{pmatrix}, \quad (\text{S6})$$

with the basis  $\mathbf{c}_i = (c_{i,a,\uparrow}, c_{i,b,\uparrow}, c_{i,a,\downarrow}, c_{i,b,\downarrow})^T$  and

$$H_{0;ij} = \sum_{\nu=0,x,y,z} A_{ij}^\nu s_\nu, \quad (\text{S7})$$

$$\Delta_{ij} = i \left\{ \Delta_0 \delta_{ij} + \frac{\Delta_s}{2} (\delta_{j,i+\hat{x}} + \delta_{j,i-\hat{x}} + \delta_{j,i+\hat{y}} + \delta_{j,i-\hat{y}}) \right\} \sigma_0 s_y, \quad (\text{S8})$$

where

$$A_{ij}^0 = \left\{ m_0 \delta_{ij} - t \sum_{\nu=x,y,z} (\delta_{j,i+\hat{\nu}} + \delta_{j,i-\hat{\nu}}) \right\} \sigma_z - \mu \delta_{ij} \sigma_0, \quad (\text{S9})$$

$$A_{ij}^\alpha = -i\lambda (\delta_{j,i+\hat{\alpha}} - \delta_{j,i-\hat{\alpha}}) \sigma_x + h_\alpha \delta_{ij} \sigma_0, \quad (\text{S10})$$

are four  $2N \times 2N$  matrices for  $N = L_x L_y L_z$  and  $\alpha \in \{x, y, z\}$ . In the presence of a  $\pi$ -flux vortex line, let us say along  $z$  direction, we need only modify the  $\Delta_{ij}$  matrix. In this case, we should replace the site-independent real numbers

$\Delta_0$  and  $\Delta_s$  with the site-dependent complex numbers as given by,

$$\Delta_\nu \longrightarrow \Delta_\nu \tanh\left(\frac{r_\nu}{\xi}\right) e^{i\phi_\nu} = \Delta_\nu \tanh\left(\frac{r_\nu}{\xi}\right) (\cos \phi_\nu + i \sin \phi_\nu) \quad (\text{S11})$$

where  $\xi$  is the superconducting coherence length,  $\nu \in \{0, s\}$ ,  $\cos \phi_\nu = x_\nu/r_\nu$ ,  $\sin \phi_\nu = y_\nu/r_\nu$ , and  $r_\nu = \sqrt{x_\nu^2 + y_\nu^2}$ . Moreover,  $x_0 = x_i$ ,  $y_0 = y_i$ ;  $x_s = \frac{1}{2}(x_i + x_j)$ ,  $y_s = \frac{1}{2}(y_i + y_j)$ , where  $(x_i, y_i)$  and  $(x_j, y_j)$  denote two nearest-neighbor sites in the  $xy$  plane over which the  $\Delta_s$  order parameter extends. Throughout this work, the center of the vortex line is chosen to be located at the center of the  $xy$  plane. Similar forms can be adopted if one wants to study vortex lines in other places or along other directions.

### III. THE $\mathbb{Z}_2$ INVARIANT CHARACTERIZES THE SYSTEM

While the presence of a straight  $z$ -directional vortex line breaks the translational symmetry in the  $x$  and  $y$  directions, the  $z$  direction still preserves translational symmetry and  $k_z$  is still a good quantum number. Therefore, the whole system can be taken as a quasi-1D superconductor. Since the presence of a vortex line also breaks the time-reversal symmetry, this quasi-1D superconductor thus falls into the D class of the Atland-Zirnbauer classification [S1, S2]. As is known, when a superconductor in the D class is fully gapped, its band topology is characterized by a  $\mathbb{Z}_2$  invariant of the form [S3]

$$\nu = \text{sgn}\{\text{Pf}[H_M(0)]\} \cdot \text{sgn}\{\text{Pf}[H_M(\pi)]\}, \quad (\text{S12})$$

where  $H_M(k_z)$  represents the Hamiltonian in the Majorana representation, which is an antisymmetric matrix forced by the intrinsic self-adjoint property of Majorana operators; ‘‘PF’’ is a shorthand notation of Pfaffian. The formula (S12) implies that a change of the  $\mathbb{Z}_2$  invariant, or say a topological phase transition, can only occur at  $k_z = 0$  or  $\pi$ , a consequence originating from the particle-hole symmetry. To obtain the explicit form of  $H_M(k_z)$ , we introduce the following Majorana operators,

$$\gamma_{\alpha,s,\mathbf{r};1} = \frac{1}{\sqrt{2}}(c_{\alpha,s,\mathbf{r}}^\dagger + c_{\alpha,s,\mathbf{r}}) = \gamma_{\alpha,s,\mathbf{r};1}^\dagger, \quad (\text{S13})$$

$$\gamma_{\alpha,s,\mathbf{r};2} = \frac{i}{\sqrt{2}}(c_{\alpha,s,\mathbf{r}}^\dagger - c_{\alpha,s,\mathbf{r}}) = \gamma_{\alpha,s,\mathbf{r};2}^\dagger, \quad (\text{S14})$$

at orbital  $\alpha$ , with spin  $s$ , and at site  $\mathbf{r}$ . Since only the two time-reversal invariant momenta are relevant for the determination of the underlying band topology, in the following we restrict ourselves to these two points. At  $k_z = 0$ , it is straightforward to find that the real space Hamiltonian is reduced as

$$\begin{aligned} H(k_z = 0) = & \sum_{\bar{\mathbf{r}}; \alpha\alpha'; s, s'} \left\{ -\mu c_{\alpha,s,\bar{\mathbf{r}}}^\dagger \delta_{\alpha\alpha'} \delta_{ss'} c_{\alpha',s',\bar{\mathbf{r}}} + (m_0 - 2t) c_{\alpha,s,\bar{\mathbf{r}}}^\dagger [\sigma_z]_{\alpha\alpha'} \delta_{ss'} c_{\alpha',s',\bar{\mathbf{r}}} + h_z c_{\alpha,s,\bar{\mathbf{r}}}^\dagger \delta_{\alpha\alpha'} [s_z]_{ss'} c_{\alpha',s',\bar{\mathbf{r}}} \right. \\ & - (t c_{\alpha,s,\bar{\mathbf{r}}}^\dagger [\sigma_z]_{\alpha\alpha'} \delta_{ss'} c_{\alpha',s',\bar{\mathbf{r}}+\hat{\mathbf{x}}} + t c_{\alpha,s,\bar{\mathbf{r}}}^\dagger [\sigma_z]_{\alpha\alpha'} \delta_{ss'} c_{\alpha',s',\bar{\mathbf{r}}+\hat{\mathbf{y}}} + h.c.) \\ & + (-i\lambda c_{\alpha,s,\bar{\mathbf{r}}}^\dagger [\sigma_x]_{\alpha\alpha'} [s_x]_{ss'} c_{\alpha',s',\bar{\mathbf{r}}+\hat{\mathbf{x}}} - i\lambda c_{\alpha,s,\bar{\mathbf{r}}}^\dagger [\sigma_x]_{\alpha\alpha'} [s_y]_{ss'} c_{\alpha',s',\bar{\mathbf{r}}+\hat{\mathbf{y}}} + h.c.) \\ & + (i\frac{\Delta_0(\bar{\mathbf{r}})}{2} c_{\alpha,s,\bar{\mathbf{r}}}^\dagger \delta_{\alpha\alpha'} [s_y]_{ss'} c_{\alpha',s',\bar{\mathbf{r}}} + i(\frac{\Delta_1(\bar{\mathbf{r}} + \frac{\hat{\mathbf{x}}}{2})}{2} c_{\alpha,s,\bar{\mathbf{r}}}^\dagger \delta_{\alpha\alpha'} [s_y]_{ss'} c_{\alpha',s',\bar{\mathbf{r}}+\hat{\mathbf{x}}} \\ & \left. + \frac{\Delta_1(\bar{\mathbf{r}} + \frac{\hat{\mathbf{y}}}{2})}{2} c_{\alpha,s,\bar{\mathbf{r}}}^\dagger \delta_{\alpha\alpha'} [s_y]_{ss'} c_{\alpha',s',\bar{\mathbf{r}}+\hat{\mathbf{y}}} + h.c.) \right\}, \quad (\text{S15}) \end{aligned}$$

and at  $k_z = \pi$ , we have

$$\begin{aligned} H(k_z = \pi) = & \sum_{\bar{\mathbf{r}}; \alpha\alpha'; s, s'} \left\{ -\mu c_{\alpha,s,\bar{\mathbf{r}}}^\dagger \delta_{\alpha\alpha'} \delta_{ss'} c_{\alpha',s',\bar{\mathbf{r}}} + (m_0 + 2t) c_{\alpha,s,\bar{\mathbf{r}}}^\dagger [\sigma_z]_{\alpha\alpha'} \delta_{ss'} c_{\alpha',s',\bar{\mathbf{r}}} + h_z c_{\alpha,s,\bar{\mathbf{r}}}^\dagger \delta_{\alpha\alpha'} [s_z]_{ss'} c_{\alpha',s',\bar{\mathbf{r}}} \right. \\ & - (t c_{\alpha,s,\bar{\mathbf{r}}}^\dagger [\sigma_z]_{\alpha\alpha'} \delta_{ss'} c_{\alpha',s',\bar{\mathbf{r}}+\hat{\mathbf{x}}} + t c_{\alpha,s,\bar{\mathbf{r}}}^\dagger [\sigma_z]_{\alpha\alpha'} \delta_{ss'} c_{\alpha',s',\bar{\mathbf{r}}+\hat{\mathbf{y}}} + h.c.) \\ & + (-i\lambda c_{\alpha,s,\bar{\mathbf{r}}}^\dagger [\sigma_x]_{\alpha\alpha'} [s_x]_{ss'} c_{\alpha',s',\bar{\mathbf{r}}+\hat{\mathbf{x}}} - i\lambda c_{\alpha,s,\bar{\mathbf{r}}}^\dagger [\sigma_x]_{\alpha\alpha'} [s_y]_{ss'} c_{\alpha',s',\bar{\mathbf{r}}+\hat{\mathbf{y}}} + h.c.) \\ & + (i\frac{\Delta_0(\bar{\mathbf{r}})}{2} c_{\alpha,s,\bar{\mathbf{r}}}^\dagger \delta_{\alpha\alpha'} [s_y]_{ss'} c_{\alpha',s',\bar{\mathbf{r}}} + i(\frac{\Delta_1(\bar{\mathbf{r}} + \frac{\hat{\mathbf{x}}}{2})}{2} c_{\alpha,s,\bar{\mathbf{r}}}^\dagger \delta_{\alpha\alpha'} [s_y]_{ss'} c_{\alpha',s',\bar{\mathbf{r}}+\hat{\mathbf{x}}} \\ & \left. + \frac{\Delta_1(\bar{\mathbf{r}} + \frac{\hat{\mathbf{y}}}{2})}{2} c_{\alpha,s,\bar{\mathbf{r}}}^\dagger \delta_{\alpha\alpha'} [s_y]_{ss'} c_{\alpha',s',\bar{\mathbf{r}}+\hat{\mathbf{y}}} + h.c.) \right\}, \quad (\text{S16}) \end{aligned}$$

where  $\bar{\mathbf{r}} = (x, y)$  only involves the lattice sites because the kinetic terms in the  $z$  direction have been rewritten in the momentum space due to the preservation of translational symmetry in this direction. It is worth noting that because the vortex line is generated along the  $z$  direction, above we have accordingly taken  $\mathbf{h} = (0, 0, h_z)$ . Substituting the Dirac fermion operators by Majorana operators, we get

$$\begin{aligned}
H(k_z = 0) = & \sum_{\bar{\mathbf{r}}; \alpha\alpha'; s, s'} \left\{ -i\mu\gamma_{\alpha, s, \bar{\mathbf{r}}; 1} \delta_{\alpha\alpha'} \delta_{ss'} \gamma_{\alpha', s', \bar{\mathbf{r}}; 2} + i(m - 2t)\gamma_{\alpha, s, \bar{\mathbf{r}}; 1} [\sigma_z]_{\alpha\alpha'} \delta_{ss'} \gamma_{\alpha', s', \bar{\mathbf{r}}; 2} \right. \\
& + ih_z \gamma_{\alpha, s, \bar{\mathbf{r}}; 1} \delta_{\alpha\alpha'} [\sigma_z]_{ss'} \gamma_{\alpha', s', \bar{\mathbf{r}}; 2} - it(\gamma_{\alpha, s, \bar{\mathbf{r}}; 1} [\sigma_z]_{\alpha\alpha'} \delta_{ss'} \gamma_{\alpha', s', \bar{\mathbf{r}} + \hat{\mathbf{x}}; 2} - \gamma_{\alpha, s, \bar{\mathbf{r}}; 2} [\sigma_z]_{\alpha\alpha'} \delta_{ss'} \gamma_{\alpha', s', \bar{\mathbf{r}} + \hat{\mathbf{x}}; 1}) \\
& - it(\gamma_{\alpha, s, \bar{\mathbf{r}}; 1} [\sigma_z]_{\alpha\alpha'} \delta_{ss'} \gamma_{\alpha', s', \bar{\mathbf{r}} + \hat{\mathbf{y}}; 2} - \gamma_{\alpha, s, \bar{\mathbf{r}}; 2} [\sigma_z]_{\alpha\alpha'} \delta_{ss'} \gamma_{\alpha', s', \bar{\mathbf{r}} + \hat{\mathbf{y}}; 1}) \\
& - i\lambda(\gamma_{\alpha, s, \bar{\mathbf{r}}; 1} [\sigma_x]_{\alpha\alpha'} [\sigma_x]_{ss'} \gamma_{\alpha', s', \bar{\mathbf{r}} + \hat{\mathbf{x}}; 1} + \gamma_{\alpha, s, \bar{\mathbf{r}}; 2} [\sigma_x]_{\alpha\alpha'} [\sigma_x]_{ss'} \gamma_{\alpha', s', \bar{\mathbf{r}} + \hat{\mathbf{x}}; 2}) \\
& + \lambda(\gamma_{\alpha, s, \bar{\mathbf{r}}; 1} [\sigma_y]_{\alpha\alpha'} [\sigma_y]_{ss'} \gamma_{\alpha', s', \bar{\mathbf{r}} + \hat{\mathbf{y}}; 2} - \gamma_{\alpha, s, \bar{\mathbf{r}}; 2} [\sigma_x]_{\alpha\alpha'} [\sigma_x]_{ss'} \gamma_{\alpha', s', \bar{\mathbf{r}} + \hat{\mathbf{y}}; 1}) \\
& + \frac{\text{Re}\Delta_0(\bar{\mathbf{r}})}{2} (\gamma_{\alpha, s, \bar{\mathbf{r}}; 2} \delta_{\alpha\alpha'} [\sigma_y]_{ss'} \gamma_{\alpha', s', \bar{\mathbf{r}}; 1} + \gamma_{\alpha, s, \bar{\mathbf{r}}; 1} \delta_{\alpha\alpha'} [\sigma_y]_{ss'} \gamma_{\alpha', s', \bar{\mathbf{r}}; 2}) \\
& - \frac{\text{Im}\Delta_0(\bar{\mathbf{r}})}{2} (\gamma_{\alpha, s, \bar{\mathbf{r}}; 1} \delta_{\alpha\alpha'} [\sigma_y]_{ss'} \gamma_{\alpha', s', \bar{\mathbf{r}}; 1} - \gamma_{\alpha, s, \bar{\mathbf{r}}; 2} \delta_{\alpha\alpha'} [\sigma_y]_{ss'} \gamma_{\alpha', s', \bar{\mathbf{r}}; 2}) \\
& + \frac{\text{Re}\Delta_1(\bar{\mathbf{r}} + \frac{\hat{\mathbf{x}}}{2})}{2} (\gamma_{\alpha, s, \bar{\mathbf{r}}; 2} \delta_{\alpha\alpha'} [\sigma_y]_{ss'} \gamma_{\alpha', s', \bar{\mathbf{r}} + \hat{\mathbf{x}}; 1} + \gamma_{\alpha, s, \bar{\mathbf{r}}; 1} \delta_{\alpha\alpha'} [\sigma_y]_{ss'} \gamma_{\alpha', s', \bar{\mathbf{r}} + \hat{\mathbf{x}}; 2}) \\
& - \frac{\text{Im}\Delta_1(\bar{\mathbf{r}} + \frac{\hat{\mathbf{x}}}{2})}{2} (\gamma_{\alpha, s, \bar{\mathbf{r}}; 1} \delta_{\alpha\alpha'} [\sigma_y]_{ss'} \gamma_{\alpha', s', \bar{\mathbf{r}} + \hat{\mathbf{x}}; 1} - \gamma_{\alpha, s, \bar{\mathbf{r}}; 2} \delta_{\alpha\alpha'} [\sigma_y]_{ss'} \gamma_{\alpha', s', \bar{\mathbf{r}} + \hat{\mathbf{x}}; 2}) \\
& + \frac{\text{Re}\Delta_1(\bar{\mathbf{r}} + \frac{\hat{\mathbf{y}}}{2})}{2} (\gamma_{\alpha, s, \bar{\mathbf{r}}; 2} \delta_{\alpha\alpha'} [\sigma_y]_{ss'} \gamma_{\alpha', s', \bar{\mathbf{r}} + \hat{\mathbf{y}}; 1} + \gamma_{\alpha, s, \bar{\mathbf{r}}; 1} \delta_{\alpha\alpha'} [\sigma_y]_{ss'} \gamma_{\alpha', s', \bar{\mathbf{r}} + \hat{\mathbf{y}}; 2}) \\
& \left. - \frac{\text{Im}\Delta_1(\bar{\mathbf{r}} + \frac{\hat{\mathbf{y}}}{2})}{2} (\gamma_{\alpha, s, \bar{\mathbf{r}}; 1} \delta_{\alpha\alpha'} [\sigma_y]_{ss'} \gamma_{\alpha', s', \bar{\mathbf{r}} + \hat{\mathbf{y}}; 1} - \gamma_{\alpha, s, \bar{\mathbf{r}}; 2} \delta_{\alpha\alpha'} [\sigma_y]_{ss'} \gamma_{\alpha', s', \bar{\mathbf{r}} + \hat{\mathbf{y}}; 2}) \right\}. \tag{S17}
\end{aligned}$$

and

$$\begin{aligned}
H(k_z = \pi) = & \sum_{\bar{\mathbf{r}}; \alpha\alpha'; s, s'} \left\{ -i\mu\gamma_{\alpha, s, \bar{\mathbf{r}}; 1} \delta_{\alpha\alpha'} \delta_{ss'} \gamma_{\alpha', s', \bar{\mathbf{r}}; 2} + i(m + 2t)\gamma_{\alpha, s, \bar{\mathbf{r}}; 1} [\sigma_z]_{\alpha\alpha'} \delta_{ss'} \gamma_{\alpha', s', \bar{\mathbf{r}}; 2} \right. \\
& + ih_z \gamma_{\alpha, s, \bar{\mathbf{r}}; 1} \delta_{\alpha\alpha'} [\sigma_z]_{ss'} \gamma_{\alpha', s', \bar{\mathbf{r}}; 2} - it(\gamma_{\alpha, s, \bar{\mathbf{r}}; 1} [\sigma_z]_{\alpha\alpha'} \delta_{ss'} \gamma_{\alpha', s', \bar{\mathbf{r}} + \hat{\mathbf{x}}; 2} - \gamma_{\alpha, s, \bar{\mathbf{r}}; 2} [\sigma_z]_{\alpha\alpha'} \delta_{ss'} \gamma_{\alpha', s', \bar{\mathbf{r}} + \hat{\mathbf{x}}; 1}) \\
& - it(\gamma_{\alpha, s, \bar{\mathbf{r}}; 1} [\sigma_z]_{\alpha\alpha'} \delta_{ss'} \gamma_{\alpha', s', \bar{\mathbf{r}} + \hat{\mathbf{y}}; 2} - \gamma_{\alpha, s, \bar{\mathbf{r}}; 2} [\sigma_z]_{\alpha\alpha'} \delta_{ss'} \gamma_{\alpha', s', \bar{\mathbf{r}} + \hat{\mathbf{y}}; 1}) \\
& - i\lambda(\gamma_{\alpha, s, \bar{\mathbf{r}}; 1} [\sigma_x]_{\alpha\alpha'} [\sigma_x]_{ss'} \gamma_{\alpha', s', \bar{\mathbf{r}} + \hat{\mathbf{x}}; 1} + \gamma_{\alpha, s, \bar{\mathbf{r}}; 2} [\sigma_x]_{\alpha\alpha'} [\sigma_x]_{ss'} \gamma_{\alpha', s', \bar{\mathbf{r}} + \hat{\mathbf{x}}; 2}) \\
& + \lambda(\gamma_{\alpha, s, \bar{\mathbf{r}}; 1} [\sigma_x]_{\alpha\alpha'} [\sigma_y]_{ss'} \gamma_{\alpha', s', \bar{\mathbf{r}} + \hat{\mathbf{y}}; 2} - \gamma_{\alpha, s, \bar{\mathbf{r}}; 2} [\sigma_x]_{\alpha\alpha'} [\sigma_y]_{ss'} \gamma_{\alpha', s', \bar{\mathbf{r}} + \hat{\mathbf{y}}; 1}) \\
& + \frac{\text{Re}\Delta_0(\bar{\mathbf{r}})}{2} (\gamma_{\alpha, s, \bar{\mathbf{r}}; 2} \delta_{\alpha\alpha'} [\sigma_y]_{ss'} \gamma_{\alpha', s', \bar{\mathbf{r}}; 1} + \gamma_{\alpha, s, \bar{\mathbf{r}}; 1} \delta_{\alpha\alpha'} [\sigma_y]_{ss'} \gamma_{\alpha', s', \bar{\mathbf{r}}; 2}) \\
& - \frac{\text{Im}\Delta_0(\bar{\mathbf{r}})}{2} (\gamma_{\alpha, s, \bar{\mathbf{r}}; 1} \delta_{\alpha\alpha'} [\sigma_y]_{ss'} \gamma_{\alpha', s', \bar{\mathbf{r}}; 1} - \gamma_{\alpha, s, \bar{\mathbf{r}}; 2} \delta_{\alpha\alpha'} [\sigma_y]_{ss'} \gamma_{\alpha', s', \bar{\mathbf{r}}; 2}) \\
& + \frac{\text{Re}\Delta_1(\bar{\mathbf{r}} + \frac{\hat{\mathbf{x}}}{2})}{2} (\gamma_{\alpha, s, \bar{\mathbf{r}}; 2} \delta_{\alpha\alpha'} [\sigma_y]_{ss'} \gamma_{\alpha', s', \bar{\mathbf{r}} + \hat{\mathbf{x}}; 1} + \gamma_{\alpha, s, \bar{\mathbf{r}}; 1} \delta_{\alpha\alpha'} [\sigma_y]_{ss'} \gamma_{\alpha', s', \bar{\mathbf{r}} + \hat{\mathbf{x}}; 2}) \\
& - \frac{\text{Im}\Delta_1(\bar{\mathbf{r}} + \frac{\hat{\mathbf{x}}}{2})}{2} (\gamma_{\alpha, s, \bar{\mathbf{r}}; 1} \delta_{\alpha\alpha'} [\sigma_y]_{ss'} \gamma_{\alpha', s', \bar{\mathbf{r}} + \hat{\mathbf{x}}; 1} - \gamma_{\alpha, s, \bar{\mathbf{r}}; 2} \delta_{\alpha\alpha'} [\sigma_y]_{ss'} \gamma_{\alpha', s', \bar{\mathbf{r}} + \hat{\mathbf{x}}; 2}) \\
& + \frac{\text{Re}\Delta_1(\bar{\mathbf{r}} + \frac{\hat{\mathbf{y}}}{2})}{2} (\gamma_{\alpha, s, \bar{\mathbf{r}}; 2} \delta_{\alpha\alpha'} [\sigma_y]_{ss'} \gamma_{\alpha', s', \bar{\mathbf{r}} + \hat{\mathbf{y}}; 1} + \gamma_{\alpha, s, \bar{\mathbf{r}}; 1} \delta_{\alpha\alpha'} [\sigma_y]_{ss'} \gamma_{\alpha', s', \bar{\mathbf{r}} + \hat{\mathbf{y}}; 2}) \\
& \left. - \frac{\text{Im}\Delta_1(\bar{\mathbf{r}} + \frac{\hat{\mathbf{y}}}{2})}{2} (\gamma_{\alpha, s, \bar{\mathbf{r}}; 1} \delta_{\alpha\alpha'} [\sigma_y]_{ss'} \gamma_{\alpha', s', \bar{\mathbf{r}} + \hat{\mathbf{y}}; 1} - \gamma_{\alpha, s, \bar{\mathbf{r}}; 2} \delta_{\alpha\alpha'} [\sigma_y]_{ss'} \gamma_{\alpha', s', \bar{\mathbf{r}} + \hat{\mathbf{y}}; 2}) \right\}. \tag{S18}
\end{aligned}$$

Let us consider a system with open boundary conditions in the both  $x$  and  $y$  directions where the number of lattice sites is  $N_x$  in the  $x$  direction and  $N_y$  in the  $y$  direction. In terms of the Majorana representation  $\gamma_{k_z=0/\pi} = (\Gamma_{1,1}, \Gamma_{2,1}, \dots, \Gamma_{n,m}, \dots, \Gamma_{N_x, N_y})^T$  with  $\Gamma_{n,m} = (\gamma_{a,\uparrow, n\hat{\mathbf{x}}+m\hat{\mathbf{y}}; 1}, \gamma_{a,\uparrow, n\hat{\mathbf{x}}+m\hat{\mathbf{y}}; 2}, \gamma_{b,\uparrow, n\hat{\mathbf{x}}+m\hat{\mathbf{y}}; 1}, \gamma_{b,\uparrow, n\hat{\mathbf{x}}+m\hat{\mathbf{y}}; 2}, \gamma_{a,\downarrow, n\hat{\mathbf{x}}+m\hat{\mathbf{y}}; 1}, \gamma_{a,\downarrow, n\hat{\mathbf{x}}+m\hat{\mathbf{y}}; 2}, \gamma_{b,\downarrow, n\hat{\mathbf{x}}+m\hat{\mathbf{y}}; 1}, \gamma_{b,\downarrow, n\hat{\mathbf{x}}+m\hat{\mathbf{y}}; 2})$ , the Hamiltonian can be written as

$$H(k_z = 0/\pi) = i\gamma_{0/\pi}^\dagger H_M(k_x = 0/\pi) \gamma_{0/\pi}, \tag{S19}$$

where  $H_M$  is an  $8N_x N_y \times 8N_x N_y$  real antisymmetric matrix for which the Pfaffian is well defined. In this work, the Pfaffian has been calculated by using the code developed in Ref. [S4]

#### IV. THE EFFECTS OF ZEEMAN FIELD ON THE HELICAL MAJORANA HINGE MODES

In the main article, we showed that in the absence of a Zeeman field, the Majorana hinge modes are helical due to the preservation of time-reversal symmetry. In this section, we show the impact of the Zeeman field on the Majorana hinge modes in detail. Naively, one may expect that the introduction of Zeeman field would immediately gap the helical Majorana hinge modes due to the breaking of time-reversal symmetry. However, the actual results are in contradiction with this expectation.

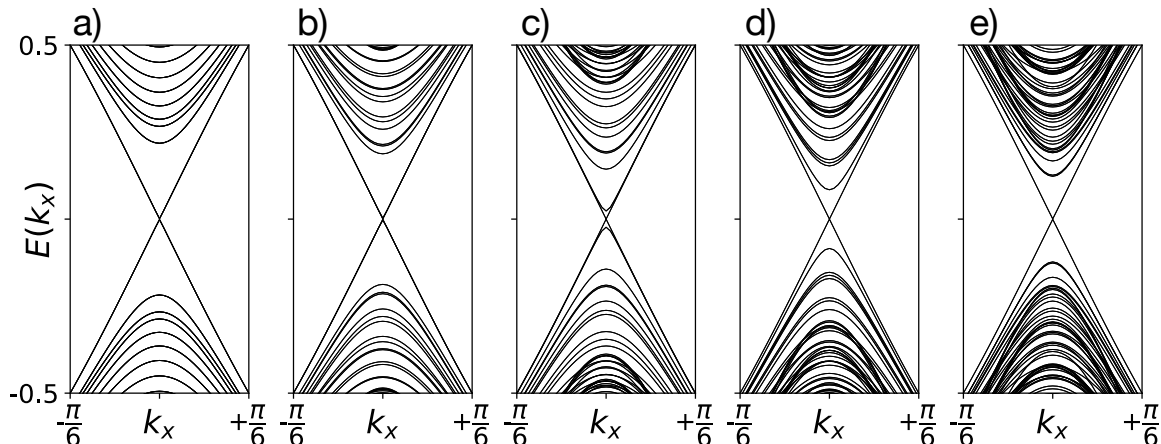


FIG. S2. Common parameters are  $t = 1$ ,  $m_0 = 2.5$ ,  $\lambda = 0.5$ ,  $\mu = 0$ ,  $\Delta_0 = -\Delta_s = 0.25$ ,  $h_x = h_y = 0$ . The lengths along the  $y$  and  $z$  directions are  $L_y = L_z = 24$ . (a)  $h_z = 0$ , (b)  $h_z = 0.1$ , (c)  $h_z = 0.2$ , (d)  $h_z = 0.3$ , (e)  $h_z = 0.4$ . In (a) (b), the gapless modes traversing the gap are of four-fold degeneracy, corresponding to four-pairs of helical Majorana hinge modes. (c) shows the spectra just crossing the transition from a second-order topological superconductor with helical Majorana hinge modes to a second-order topological superconductor with chiral Majorana hinge modes. In (d) (e), the gapless modes traversing the gap are of two-fold degeneracy, corresponding to four-branches of chiral Majorana hinge modes.

In Fig. S2 and Fig. S3, we show the evolution of the energy spectra with respect to Zeeman field. The underlying cubic geometry takes an open boundary condition in the  $y$  and  $z$  directions and periodic boundary condition in the  $x$  direction. In Fig. S2, the magnetic field is applied in the  $z$  direction *i.e.*  $\mathbf{h} = (0, 0, h_z)$ , and in Fig. S3, the magnetic field is applied in the  $[111]$  direction *i.e.*  $\mathbf{h} = (h, h, h)$ . For comparison, the result for the time-reversal invariant

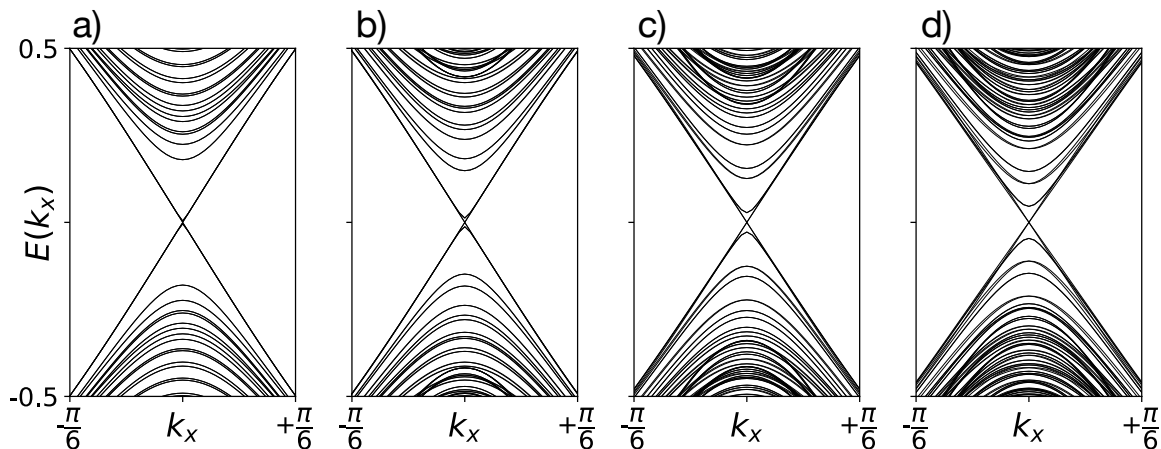


FIG. S3. Common parameters are  $t = 1$ ,  $m_0 = 2.5$ ,  $\lambda = 0.5$ ,  $\mu = 0$ ,  $\Delta_0 = -\Delta_s = 0.25$ . The lengths along the  $y$  and  $z$  directions are  $L_y = L_z = 24$ .  $\mathbf{h} = (h, h, h)$ , with (a)  $h = 0.05$ , (b)  $h = 0.1$ , (c)  $h = 0.15$ , (d)  $h = 0.2$ . In (a) (b), the gapless modes traversing the gap are of four-fold degenerate, corresponding to four-pairs of helical Majorana hinge modes. (c) shows the spectra just crossing the transition from a second-order topological superconductor with helical Majorana hinge modes to a second-order topological superconductor with chiral Majorana hinge modes. In (d), the gapless modes traversing the gap are of two-fold degenerate, corresponding to four-branches of chiral Majorana hinge modes.

case ( $\mathbf{h} = 0$ ) is presented in Fig. S2(a). In Fig. S2(b) and Fig. S3(a), one can see that the Majorana hinge modes remain gapless in a small applied field. Moreover, the degeneracy of the Majorana hinge modes does not change even though the degeneracy of other higher-energy spectra is lifted due to the breaking of time-reversal symmetry. The helical Majorana hinge modes are found to remain intact until the Zeeman field becomes larger than an orientation-dependent critical value. In Fig. S2(c) and Fig. S3(b), the results show that when the Zeeman field becomes a little larger than the critical value, half of the gapless Majorana hinge modes become gapped. We find that this corresponds to a transition from a second-order topological superconductor with helical Majorana hinge modes to a second-order topological superconductor with chiral Majorana hinge modes. With a further increase of Zeeman field, these chiral Majorana hinge modes become more separated from other modes in energy, as shown in Figs. S2(d) and S2(e) and Figs. S3(c) and S3(d).

In the following, we develop an analytic theory to explain the robustness of helical Majorana hinge modes against the Zeeman field. Following the standard procedure, we first perform a lower-energy expansion of the lattice Hamiltonian in Eq. (1) of the main article around the band-inversion momentum. Without loss of generality, we still consider that the band inversion occurs at the  $\Gamma$  point. Accordingly, the low-energy continuum Hamiltonian reads

$$\mathcal{H}(\mathbf{k}) = (m + tk^2)\sigma_z s_0 \tau_z + 2\lambda\sigma_x \mathbf{k} \cdot \mathbf{s} \tau_z - \mu\sigma_0 s_0 \tau_z + \sigma_0 \mathbf{h} \cdot \mathbf{s} \tau_0 - [\Delta_0 + 2\Delta_s - \frac{\Delta_s}{2}(k_x^2 + k_y^2)]\sigma_0 s_0 \tau_x, \quad (\text{S20})$$

where  $m = m_0 - 6t$ . For simplicity, we focus on  $\mu = 0$  in the following and take  $t$  and  $\lambda$  to be positive. Let us first derive the low-energy Hamiltonian for the surface states on the  $z$ -normal surfaces. To proceed, let us consider a semi-infinity sample with  $0 \leq z < +\infty$ . The presence of a boundary breaks the translational symmetry in the  $z$  direction, so the  $k_z$  in Hamiltonian (S20) needs to be replaced by  $-i\partial_z$ . Following Ref. [S5], we divide the Hamiltonian into two parts,  $\mathcal{H} = \mathcal{H}_1 + \mathcal{H}_2$ , where

$$\begin{aligned} \mathcal{H}_1(k_x, k_y, -i\partial_z) &= [m + t(k_x^2 + k_y^2) - t\partial_z^2]\sigma_z s_0 \tau_z - 2i\lambda\partial_z \sigma_x s_z \tau_z. \\ \mathcal{H}_2(k_x, k_y, -i\partial_z) &= 2\lambda\sigma_x(k_x s_x + k_y s_y)\tau_z + \sigma_0 \mathbf{h} \cdot \mathbf{s} \tau_0 - [\Delta_0 + 2\Delta_s - \frac{\Delta_s}{2}(k_x^2 + k_y^2)]\sigma_0 s_0 \tau_x. \end{aligned} \quad (\text{S21})$$

In the division, we have taken  $\mathcal{H}_2$  as a perturbation, which is quite accurate when the pairing amplitude and the strength of Zeeman field are small. By solving the eigenvalue equation  $\mathcal{H}_1(k_x, k_y, -i\partial_z)\psi_\alpha(z) = E_\alpha\psi_\alpha(z)$  with the boundary condition  $\psi_\alpha(0) = \psi_\alpha(+\infty) = 0$ , one can find that there exist four zero-energy solutions. The wave functions  $\psi_\alpha(z)$  can be compactly written as

$$\psi_\alpha(z) = \mathcal{N} \sin(\kappa_1 z) e^{-\kappa_2 z} e^{ik_x x} e^{ik_y y} \chi_\alpha, \quad (\text{S22})$$

with normalization given by  $|\mathcal{N}|^2 = |4\kappa_2(\kappa_1^2 + \kappa_2^2)/\kappa_1^2|$ . The two parameters  $\kappa_1$  and  $\kappa_2$  are respectively given by  $\kappa_1 = \sqrt{\frac{[t(k_x^2 + k_y^2) - m]}{t} - (\frac{\lambda}{t})^2}$  and  $\kappa_2 = \frac{\lambda}{t}$ . The most important information is contained in  $\chi_\alpha$ . Here  $\chi_\alpha$  satisfy  $\sigma_x s_z \tau_0 \chi_\alpha = -\chi_\alpha$ . We can explicitly choose solutions as

$$\begin{aligned} \chi_1 &= |\sigma_y = -1\rangle \otimes |s_z = 1\rangle \otimes |\tau_z = 1\rangle, \\ \chi_2 &= |\sigma_y = 1\rangle \otimes |s_z = -1\rangle \otimes |\tau_z = 1\rangle, \\ \chi_3 &= |\sigma_y = -1\rangle \otimes |s_z = 1\rangle \otimes |\tau_z = -1\rangle, \\ \chi_4 &= |\sigma_y = 1\rangle \otimes |s_z = -1\rangle \otimes |\tau_z = -1\rangle. \end{aligned} \quad (\text{S23})$$

By projecting  $\mathcal{H}_2$  into the four-dimensional space expanded by  $\chi_\alpha$ , we obtain the low-energy Hamiltonian for the surface states on the  $z = 0$  surface, which reads

$$\mathcal{H}_{\text{eff}}(k_x, k_y) = 2\lambda(k_y s_x - k_x s_y)\tau_z + M_Z s_z + M_S \tau_x, \quad (\text{S24})$$

where  $M_z = h_z$  denotes the Dirac mass induced by the Zeeman field, and  $M_S = \Delta_0 + 2\Delta_s$  in the leading order denotes the Dirac mass induced by the superconductivity. It is easy to see that for the Zeeman field, only the component perpendicular to the concerned surface contributes to the Dirac mass. It is worth noting that the two Dirac mass terms commute with each other, and a closure of the surface gap happens at  $M_Z = M_S$ .

With Eq. (S24), now we can explain why the helical Majorana hinge modes are stable against the Zeeman field when its strength is below the critical value. To proceed, let us consider that the  $y$  direction also becomes open and a domain wall hosting Majorana helical modes is formed at the boundary. Following the same steps, we divide the Hamiltonian (S24) into two parts,  $\mathcal{H}_{\text{eff}} = \mathcal{H}_{\text{eff};1} + \mathcal{H}_{\text{eff};2}$ , where

$$\begin{aligned} \mathcal{H}_{\text{eff};1}(k_x, -i\partial_y) &= -2i\lambda\partial_y s_x \tau_z + M_S(y)\tau_x, \\ \mathcal{H}_{\text{eff};2}(k_x, k_y) &= -2\lambda k_x s_y \tau_z + M_Z s_z. \end{aligned} \quad (\text{S25})$$

As explained previously, such a division is justified when the Zeeman field, so  $M_Z$ , is small. From our analysis above, one can immediately read from  $\mathcal{H}_{\text{eff};1}$  that the space for the low-energy modes is spanned by  $\tilde{\chi}_\alpha$  which satisfy either  $s_x \tau_y \tilde{\chi}_\alpha = \tilde{\chi}_\alpha$  or  $s_x \tau_y \tilde{\chi}_\alpha = -\tilde{\chi}_\alpha$ . That is, the two-dimensional space for the helical Majorana modes is spanned either by  $(|s_x = 1\rangle \otimes |\tau_y = 1\rangle, |s_x = -1\rangle \otimes |\tau_y = -1\rangle)$  or by  $(|s_x = 1\rangle \otimes |\tau_y = -1\rangle, |s_x = -1\rangle \otimes |\tau_y = 1\rangle)$ . Projecting  $\mathcal{H}_{\text{eff};2}$  into these two possible two-dimensional spaces, one can find that the low-energy Hamiltonian on the hinge is given by

$$\mathcal{H}_h(k_x) = -2\lambda k_y s_y. \quad (\text{S26})$$

One can immediately see that in the weak field regime (the regime for which the perturbative treatment is justified), the presence of Zeeman field does not alter the helical nature, though the time-reversal symmetry is broken.

According to Eq. (S24), we know that a closure of the surface gap happens at  $M_Z = M_S$ . This indicates that when the Dirac mass term induced by the Zeeman field is equal to the one induced by superconductivity, a surface topological phase transition occurs, accompanying a change of the nature of domain walls.

## V. VORTEX LINES IN THE $x$ DIRECTION

In the main article, we have restricted ourselves to vortex lines generated in the  $z$  direction in order to be directly comparable with the experiments. Here we provide the results for vortex lines generated in the  $x$  direction for completeness. It is worth noting that because the results for vortex lines generated in the  $y$  direction are the same due to the  $C_{4z}$  rotational symmetry, we neglect them to avoid repetition.

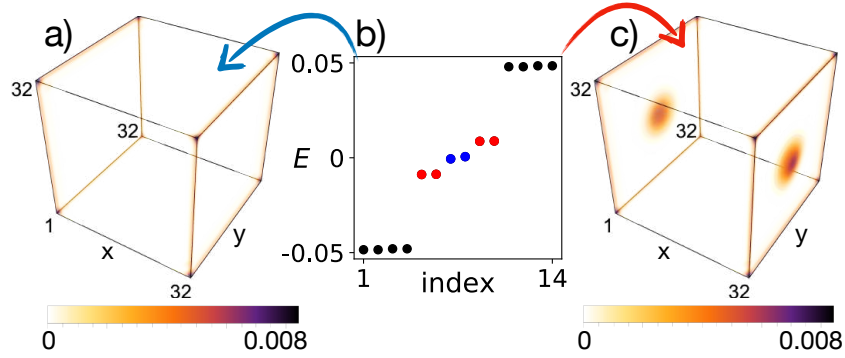


FIG. S4. (Color online) Common parameters are  $t = 1$ ,  $m_0 = 2.5$ ,  $\lambda = 0.5$ ,  $\mu = 0$ ,  $\Delta_0 = -\Delta_s = 0.25$ ,  $\xi = 4$ ,  $\mathbf{h} = 0$ . All directions take open boundary condition and their lengths are  $L_x = L_y = L_z = 32$  lattice spacings. (a) The wave functions of the Majorana zero modes [the two blue dots shown in (b)] are found to be localized at the hinges. (b) 14 energy eigenvalues closest to zero energy. (c) The wave functions of the four finite-energy modes in red color are mostly localized at the vortex ends, indicating a trivial vortex line.

Since in this work we are most interested in the interplay of vortex lines and second-order topology, here we focus on the case with a nontrivial second-order topology. As shown in Figs. S4, the results are similar to those for vortex lines generated in the  $z$  direction, indicating that the trivialization of vortex lines by the second-order topology is irrespective of the orientation of the vortex lines.

## VI. HELICAL AND CHIRAL MAJORANA HINGE MODES FOR A FINITE-SIZE CUBIC SAMPLE IN THE ABSENCE OF VORTEX LINES

In this section, we show the dispersion of Majorana hinge modes for a cubic geometry in the absence of vortex lines. As shown in Fig. S5, one can find that for the second-order topological superconducting phase with helical Majorana hinge modes, the helical Majorana hinge modes have a small but finite gap due to finite-size effects. Notably, there is no zero energy mode. Similar results are also found for the second-order topological superconducting phase with chiral Majorana hinge modes, as shown in Fig. S6. Compared with the results in the presence of a  $\pi$ -flux vortex line, these results suggest that the  $\pi$ -flux vortex line is crucial for the realization of robust Majorana zero modes on the hinges.

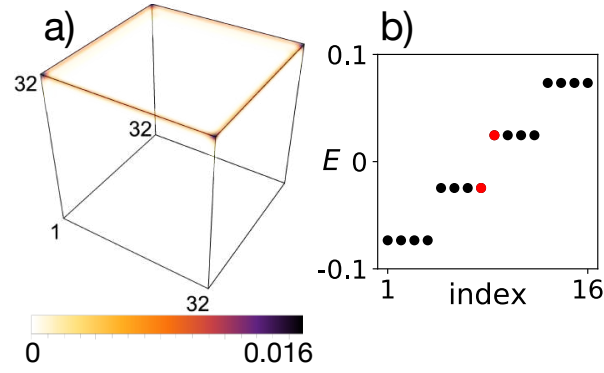


FIG. S5. (Color online) Common parameters are  $t = 1$ ,  $m_0 = 2.5$ ,  $\lambda = 0.5$ ,  $\mu = 0$ ,  $\Delta_0 = -\Delta_s = 0.25$ ,  $\mathbf{h} = 0$ . All directions take open boundary condition and their lengths are  $L_x = L_y = L_z = 32$ . (a) The density profile of the hinge states. (b) 16 energy eigenvalues closest to zero energy. No robust Majorana zero mode exists.

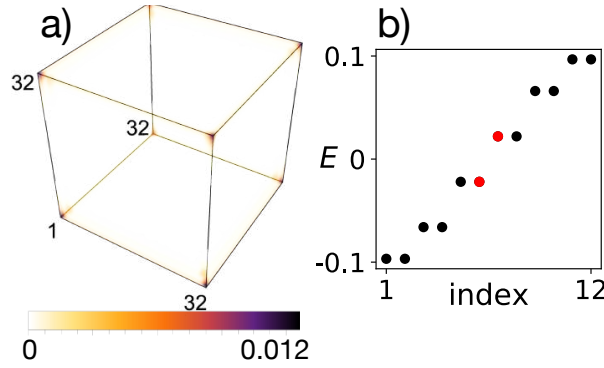


FIG. S6. (Color online) Common parameters are  $t = 1$ ,  $m_0 = 2.5$ ,  $\lambda = 0.5$ ,  $\mu = 0$ ,  $\Delta_0 = -\Delta_s = 0.25$ ,  $h_x = h_y = 0$ ,  $h_z = 0.3$ . All directions take open boundary condition and their lengths are  $L_x = L_y = L_z = 32$ . (a) The density profile of the hinge states. (b) 12 energy eigenvalues closest to zero energy. No robust Majorana zero mode exists.

\* [yanzhh5@mail.sysu.edu.cn](mailto:yanzhh5@mail.sysu.edu.cn)

- [S1] Andreas P. Schnyder, Shinsei Ryu, Akira Furusaki, and Andreas W. W. Ludwig, “Classification of topological insulators and superconductors in three spatial dimensions,” *Phys. Rev. B* **78**, 195125 (2008).
- [S2] Alexei Kitaev, “Periodic table for topological insulators and superconductors,” in *AIP Conference Proceedings*, Vol. 1134 (AIP, 2009) pp. 22–30.
- [S3] Alexei Kitaev, “Unpaired Majorana fermions in quantum wires,” *Physics-Uspekhi* **44**, 131 (2001).
- [S4] M. Wimmer, “Algorithm 923: Efficient numerical computation of the Pfaffian for dense and banded skew-symmetric matrices,” *ACM Trans. Math. Softw.* **38**, 30:1–30:17 (2012).
- [S5] Zhongbo Yan, Fei Song, and Zhong Wang, “Majorana corner modes in a high-temperature platform,” *Phys. Rev. Lett.* **121**, 096803 (2018).